

# Design of Class I/IV Bromodomain-Targeting Degraders for Chromatin Remodeling Complexes

Huda Zahid,<sup>‡,a</sup> Jeff P. Costello,<sup>‡,a</sup> Jennifer R. Kimbrough,<sup>a</sup> Marisa Actis,<sup>c</sup> Zoran Rankovic,<sup>c</sup> William C. K. Pomerantz<sup>\*,a,b</sup>

<sup>a</sup>Department of Chemistry, University of Minnesota, 207 Pleasant St. SE, Minneapolis, Minnesota 55455, United States

<sup>b</sup>Department of Medicinal Chemistry, University of Minnesota, 308 Harvard Street SE, Minneapolis, Minnesota 55455, United States

<sup>c</sup>Department of Chemical Biology & Therapeutics, St. Jude Children's Research Hospital, Memphis, TN 38105, United States

**KEYWORDS** epigenetics, chromatin remodelers, degraders, BPTF, CECR2, BRD9

---

**ABSTRACT:** Targeted protein degradation is an emerging technology that can be used for modulating the activity of epigenetic protein targets. Among bromodomain-containing proteins, a number of degraders for the BET family have been developed while non-BET bromodomains remain underexplored. Several of these proteins are subunits in chromatin remodeling complexes often associated with oncogenic roles. Here we describe the design of class I (BPTF and CECR2) and IV (BRD9) bromodomain-targeting degraders based on two scaffolds derived from pyridazinone and pyrimidine-based heterocycles. We evaluate various exit vectors and linkers to identify analogues that demonstrate selectivity within these families. We further use an in-cell NanoBRET assay to demonstrate that these heterobifunctional molecules are cell-permeable, form ternary complexes, and can degrade nanoluciferase-bromodomain fusions. Finally, as a first example of a CECR2 degrader, we observe that our pyrimidine-based analogues degrade endogenous CECR2, while showing a smaller effect on BPTF levels. The pyridazinone-based compounds did not degrade BPTF when observed through western blotting, supporting a more challenging target for degradation and a goal for future optimization.

---

## INTRODUCTION

Epigenetic regulation occurs through mechanisms that modify gene expression without changing the genomic sequence. One such process is chromatin remodeling which involves alterations in the chromatin structure through changes in the nucleosome position or histone modification, eviction, or exchange.<sup>1</sup> Remodeling can occur via both ATP-dependent and -independent mechanisms. The ATP-dependent processes are catalyzed by multidomain chromatin remodeling complexes classified into four families: SWI/SNF, ISWI, CHD and INO80.<sup>2</sup> Dysregulation of these chromatin remodelers is often associated with oncogenic phenotypes.<sup>3</sup> Several of these chromatin remodeling complexes also contain bromodomain-containing proteins. The mammalian SWI/SNF complexes BAF and PBAF contain the class IV bromodomains BRD9<sup>4</sup> and BRD7<sup>5</sup> subunits respectively. In addition, the GCN5 bromodomain stabilizes the SWI/SNF complex on chromatin.<sup>6</sup> In the less-studied ISWI family,<sup>7</sup> NURF recognizes chromatin through its largest subunit BPTF,<sup>8</sup> and CERF contains the CECR2 bromodomain-containing protein.<sup>9</sup> BPTF, CECR2 and GCN5 are members of the class I bromodomain family (**Figure 1B**) and their role in nucleosome remodeling makes them important targets for anti-cancer therapy.<sup>10</sup>

Although not as well-characterized as BET inhibitors, several small-molecule inhibitors for class I and class IV bromodomains have been recently developed.<sup>11</sup> However, for many

non-BET bromodomains, it remains unclear whether bromodomain inhibition alone will be effective to induce a significant phenotypic effect. In the case of BPTF, we<sup>12</sup> and others<sup>13</sup> have shown that bromodomain inhibitors when used as single agents may be insufficient for anticancer therapeutic applications. We previously reported that BPTF inhibitors sensitize 4T1 breast cancer cells to the chemotherapeutic, doxorubicin. Therefore, combination therapy may be a useful option in cases where bromodomain inhibition on its own proves to be ineffective.<sup>12,14</sup>

An alternative pharmacological modality is targeted protein degradation which has progressed rapidly for BET bromodomains.<sup>15</sup> In contrast, only four non-BET bromodomain targeting degraders have been reported (**Figure 1A**). These degraders have in some cases proven more effective than monovalent inhibitors. For example, the BRD9 inhibitor I-BRD9 demonstrated only modest effects in synovial sarcoma cells but a degrader generated from the same scaffold (dBRD9) led to a greater therapeutic response.<sup>16</sup> Similarly, inhibition of the highly homologous PCAF/GCN5 bromodomains by the small-molecule GSK4027 was insufficient to recapitulate the effects of genetic knockouts in macrophages, motivating the development of the degrader GSK699.<sup>17</sup> These studies highlight the significance of using protein degradation to target class I and class IV bromodomain-containing proteins. Within class I, degraders for BPTF and CECR2 have yet to be reported prior to this study.

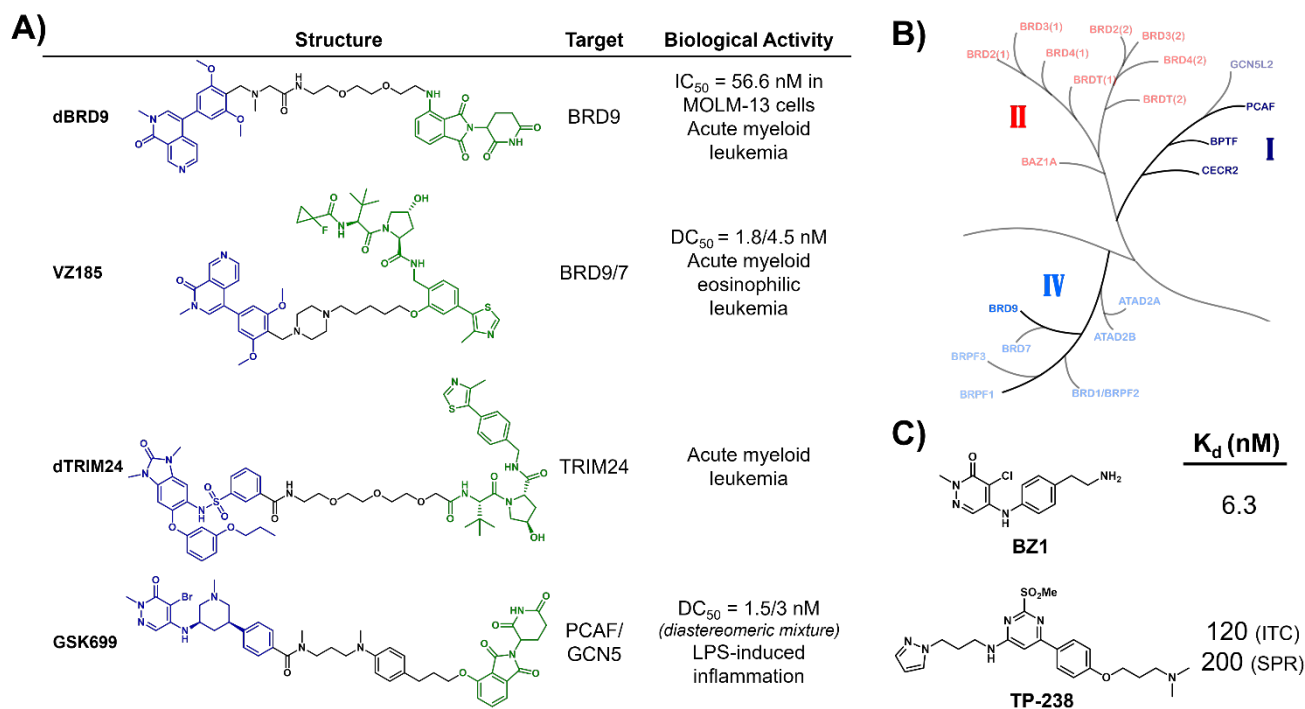


**Figure 1. A)** Previously reported non-BET bromodomain (BD) targeting degraders (bromodomain binding moiety in blue, E3 ligase ligand in green) and their biological activity. **B)** Part of the bromodomain phylogenetic tree, showing class I, II (BET), and IV bromodomains, adapted with permission from Pomerantz et al.<sup>18</sup> **C)** Pyridazinone and pyrimidine-based scaffolds with their affinity values for BPTF .

Heterobifunctional molecules also provide a new way to establish selectivity across different bromodomains. Gadd et al. showed that the BRD4 degrader MZ1 can induce protein-protein interactions with the E3 ligase leading to more stable and cooperative ternary complexes for BRD4 over other BET bromodomains.<sup>19</sup> While designing selective small-molecule inhibitors for class I bromodomains remains challenging,<sup>20</sup> forming distinct ternary complexes is a potential alternative for targeting specific members of the family.

Targeted protein degradation may also be a useful therapeutic tool given that it allows the full protein to be removed through sub-stoichiometric treatment of degrader compounds in an event-driven process. For BPTF, genetic knockdown studies have shown strong downstream phenotypic effects. Richart et al. demonstrated that BPTF knockdown resulted in decreased c-Myc recruitment to DNA.<sup>21</sup> BPTF knockdown also decreased high-grade glioma growth in adult and pediatric models.<sup>22</sup> Another class I bromodomain, CECR2, was recently shown to drive breast cancer metastasis by regulating NF- $\kappa$ B activity, making CECR2 a possible target for treating metastatic breast cancer.<sup>23</sup> Given the therapeutic utility demonstrated by genetic knockdown studies, we anticipate that protein degradation approaches would be valuable for modulating the activity of these proteins and the larger nucleosome remodeling complexes they form.

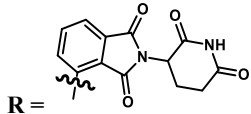
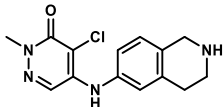
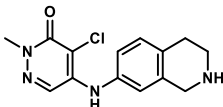
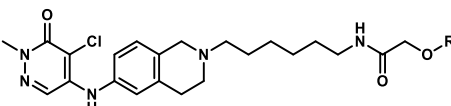
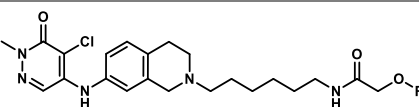
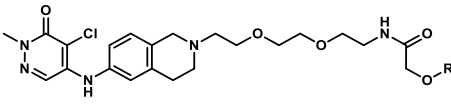
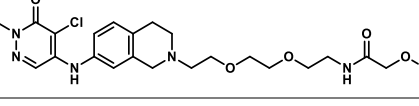
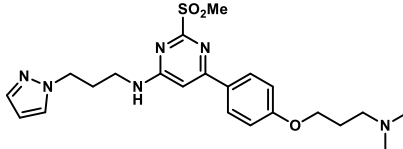
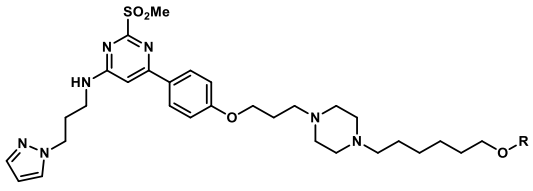
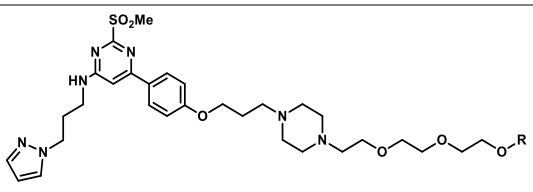
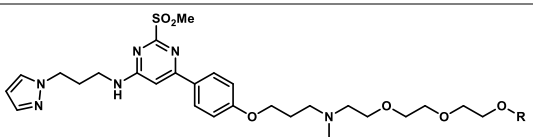
Here we describe the design and evaluation of first-generation degraders for several class I bromodomains and BRD9 in class IV using two different scaffolds (**Figure 1C**). We use a pyridazinone-based scaffold featured in BZ1, previously developed for binding to PCAF/GCN5<sup>24</sup> and BPTF,<sup>12</sup> and a pyrimidine-

based scaffold derived from TP-238, as a dual BPTF/CECR2 chemical probe.<sup>25,26</sup> We establish exit vectors for linker attachment and explore ternary complex formation through both in-vitro assays and in-cell NanoBRET. Focusing our efforts on BPTF, we use our in-cell NanoBRET assay to demonstrate degradation of a designed Nanoluciferase-bromodomain construct through both scaffolds and subsequently a full length Nanoluciferase-BRD9 construct. Finally, we show the first examples of degradation of endogenous BPTF and CECR2 using the TP-238-based degraders. Surprisingly, the pyridazinone degraders used in this study did not degrade endogenous BPTF, indicating room for further optimization. Future work will look at further structure-activity relationships (SAR) with these new degraders for tailoring selectivity and efficacy within class I bromodomains to enable subsequent cellular studies.

## RESULTS AND DISCUSSION

We previously reported compounds **1** and **2** as high affinity pyridazinone-based ligands for the BPTF bromodomain.<sup>12</sup> Through x-ray cocrystal structures, we showed that with different positions of the amine in the tetrahydroisoquinoline ring, we can engage D2957, D2960 and E2954 in BPTF (PDB: 7RWQ and 7RWO). Therefore, for our first-generation pyridazinone degraders, we chose to attach linkers from the tetrahydroisoquinoline analogues, allowing us to explore two distinct exit vectors (**Figure 2A**). We chose alkyl and PEG-based linkers to assess any potential effects on ternary complex formation and cell permeability.<sup>27</sup> Degradation **3-6** were synthesized according to **Scheme 2**, using pomalidomide-based cereblon-targeting E3 ligase ligands.

**Table 1:** AlphaScreen IC<sub>50</sub> values for inhibition of BPTF, BRD9 and CECR2 bromodomains.

		<b>BPTF BD</b> <b>IC<sub>50</sub> (nM)<sup>a</sup></b>	<b>BRD9 BD</b> <b>IC<sub>50</sub> (nM)<sup>b</sup></b>	<b>CECR2 BD</b> <b>IC<sub>50</sub> (nM)<sup>b</sup></b>
<b>1</b>		250 <sup>12</sup>	556	1670
<b>2</b>		370 <sup>12</sup>	300	1300
<b>3</b>		24 ± 9	21	53
<b>4</b>		158 ± 55	98	485
<b>5</b>		70 ± 23	63	225
<b>6</b>		121 ± 38	18	1460
<b>7</b>		430 <sup>28</sup>	ND	33
<b>8</b>		146 ± 12	844	24
<b>9</b>		267 ± 8	996	33
<b>10</b>		360 (N = 1)	ND	ND

<sup>a</sup>Average of two technical replicates with N = 3 and SD. <sup>b</sup>Average of two technical replicates with N = 2 unless otherwise indicated. ND = not determined. Binding isotherms are shown in **Figure 2C**, **Figure S1** and **S2**.

We had also reported a crystal structure of TP-238 (**7**) with BPTF (PDB ID: 7KDZ).<sup>28</sup> Overlaying the cocrystal structures of TP-238 and compound **1** (**Figure 2B**) indicated that the pendant  $N(\text{CH}_3)_2$  group in TP-238 provides a similar exit vector to the amine in compound **1**, although the longer chain in TP-238 may provide more conformational flexibility. Using TP-238, we synthesized pomalidomide conjugates **8-10** (**Scheme 5**). Compounds **8** and **9** are comprised of more rigid and polar piperazine linkers, with alkyl and PEG versions respectively. To study the effect of an alkyl linker in lieu of the piperazine ring, we designed compound **10** as the closest analogue of TP-238.

**Biophysical characterization of pyridazinone and TP-238 based degraders.** To validate our chosen exit vectors, we used an AlphaScreen assay to measure binding affinity of our degraders with the BPTF bromodomain.<sup>28</sup> Heterobifunctional molecules from both scaffolds were high affinity binders of BPTF (**Figure 1C** and **Table 1**), establishing that our exit vectors do not significantly perturb binding to the BPTF bromodomain. We further characterized the affinity of these compounds against the BRD9 and CECR2 bromodomains, which are significant off-targets of the two scaffolds (**Figure S1, Figure S2**, and **Table 1**). As observed previously with pyridazinone-based compounds, they retained binding to BRD9 and CECR2, although compound **4** and **6** demonstrated some attenuation in affinity to CECR2. Consistent with the previously reported TP-238 binding profile, our TP-238-derived conjugates displayed the highest affinity to CECR2 and in the case of **8** and **9** slightly weaker (6-8-fold) binding to BPTF.<sup>25,28</sup> In contrast to the pyridazinones, these compounds were weaker affinity binders for BRD9.<sup>25</sup> The pyridazinone and pyrimidine-based scaffolds therefore provided us with two unique selectivity profiles to target representative members of the class I and IV bromodomain families.

**In vitro ternary complex formation via AlphaScreen.** The stability of the ternary complex is critical for degradation by heterobifunctional molecules.<sup>29</sup> We therefore sought to study ternary complex formation in vitro using an AlphaScreen-based

assay (**Figure 3A**). In this experiment, glutathione-coated donor beads and nickel acceptor beads were paired with GST-tagged bromodomains (BPTF, BRD9, CECR2 and PCAF) and His-tagged CRBN-DDB1. The AlphaScreen signal was measured at varying degrader concentrations and the amplitude of the maximum point on the curve was used as an indicator of ternary complex stability. Small molecule potency was indicated by the concentration at the mid-point of the bell curve.

In this assay format, all pyridazinone-based degraders showed high ternary complex formation with BPTF (**Figure 3B**), consistent with the high affinity of the pyridazinone for this target (**Table 1**). To our surprise, while compound **4** seemed to be promiscuous, compound **3** showed a drop in signal for BRD9, CECR2 and PCAF (**Figures 3C-E**), indicating that the exit vector **1** (**Figure 2A**) in the alkyl linker series may help bias selectivity for BPTF over the other bromodomains tested in this assay. A similar albeit minor effect was observed in the PEG linker series in the case of PCAF (**Figure 3E**) but not for BRD9 or CECR2. Comparing the alkyl and PEG linkers, compounds **5** and **6** with PEG linkers generally seemed to form less stable ternary complexes for CECR2 and PCAF, compared to BPTF and BRD9. Since these compounds do not demonstrate any significant loss of affinity with the bromodomain target (**Table 1**), we hypothesize that there may be additional positive or negative cooperativity effects<sup>30</sup> during ternary complex formation contributing to this selectivity.

In contrast, we did not observe a significant difference in ternary complex stability between the alkyl and PEG linkers for the TP-238 analogues. Both compounds **8** and **9** showed similar ternary complex behavior with BPTF, BRD9 and CECR2 (**Figures 3B-D**). The signals for compound **10** were generally lower across all the proteins tested, highlighting the importance of the more rigid piperazine linker framework as opposed to alkyl chains in this scaffold. All TP-238 based degraders showed limited ternary complex formation with PCAF (**Figure 3E**). Based on these results, we focused on compounds **8** and **9** for further studies.

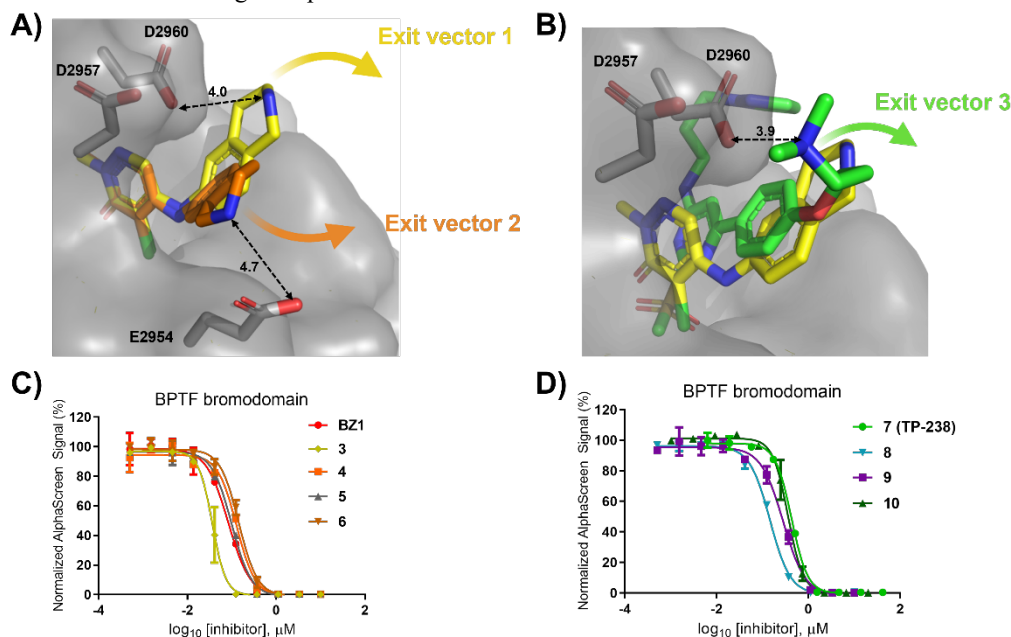


**Figure 2.** BPTF BD (gray) with **A)** compounds **1** (yellow) and **2** (orange) overlays **B)** compound **1** (yellow) and TP-238 (green) overlay. **C-D)** AlphaScreen binding isotherms for small molecules in **Table 1**, indicating BPTF bromodomain binding activity is retained.

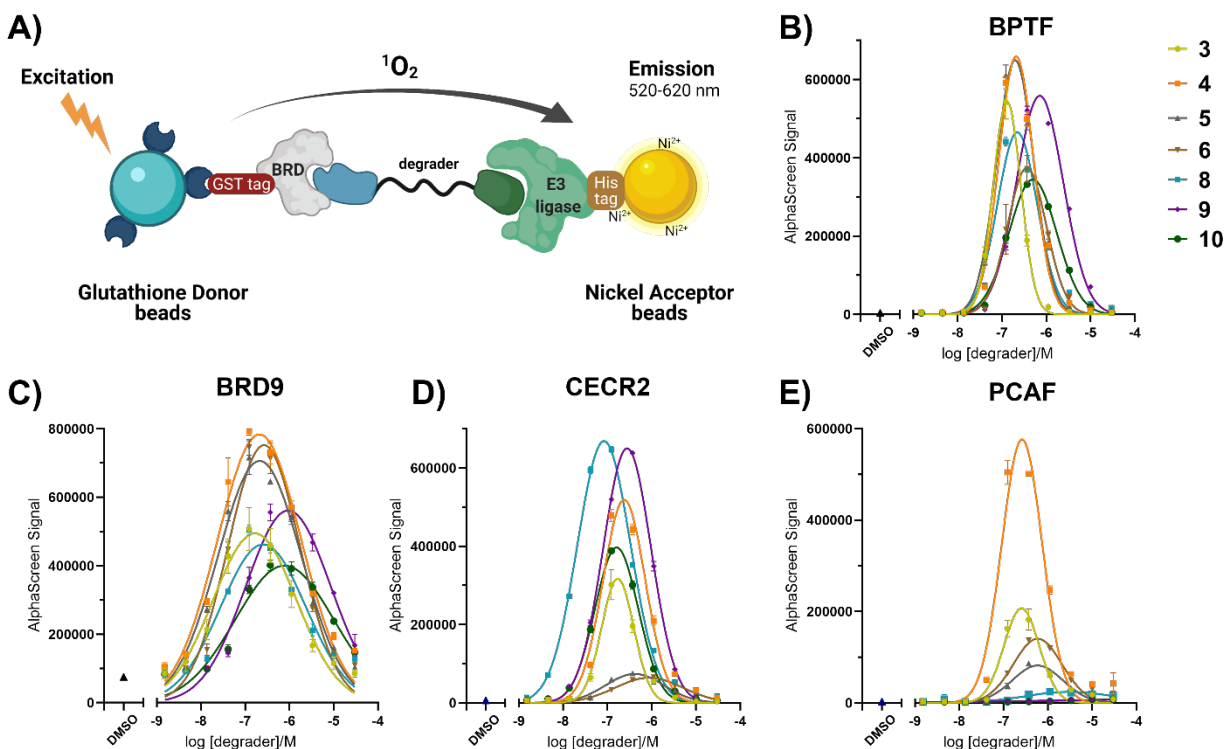


**Figure 3.** **A)** In vitro AlphaScreen ternary complex formation assay workflow. Ternary complex formation with **B)** BPTF **C)** BRD9 **D)** CECR2 **E)** PCAF bromodomains.

Comparing our pyridazinone and pyrimidine scaffolds, the pyridazinone degraders typically showed more potent ternary complex formation for BPTF and BRD9, while the TP-238 degraders were more potent for CECR2. In particular, compound **8** showed the highest potency for CECR2. This was consistent with the selectivity profile of the bromodomain-targeting moiety of these degraders. Encouragingly, apart from compound **4**, all of the other degraders demonstrated a significant loss of ternary complex stability and potency for PCAF (and most likely GCN5 due to their high sequence similarity), indicating selectivity over this important class I bromodomain target.

**In-cell ternary complex formation and degradation of BPTF-BD via NanoBRET.** After establishing in vitro ternary complex formation, we optimized a NanoBRET ternary complex assay to rank-order degraders in cells (**Figure 4A**).<sup>31</sup> This assay also serves as an indirect indicator of cellular permeability, which is often a major challenge for heterobifunctional degraders.<sup>32</sup> We designed both N- and C-terminal fusions of Nanoluciferase (Nluc) and BPTF-BD with 11-amino acid linkers (See supporting information for design of plasmid constructs). The vectors were transfected into HEK293T cells and compounds **4** and **5** were dosed at 1  $\mu$ M for 2 h in cells pre-treated with the proteasome inhibitor MG-132 to first determine ternary complex formation. We found that the C-terminal fusion construct showed ternary complex formation while the N-terminal fusion did not with either compound (**Figure S3**). We

thus used the C-terminal Nluc-BPTF-BD fusion construct for subsequent experiments.

We tested our degraders for ternary complex formation at 1  $\mu$ M (**Figure 4B**). In this assay, we observed a trend within the pyridazinone degrader series, where the alkyl linker compounds (**3** and **4**) demonstrate a higher BRET ratio (3.5- and 3.2-fold increase over DMSO respectively) compared to the PEG linkers (2.3- and 1.6-fold for compounds **5** and **6**). For the TP-238 series, a higher BRET signal was observed for compound **8** (3.1-fold over DMSO control) compared to compound **9** (1.8-fold), providing more evidence that the alkyl linkers appear to be favored. These data show that our compounds are cell-permeable in this assay, making them useful starting points for further SAR.

We then monitored the degradation of the Nluc-BPTF construct by measuring the total donor luminescence after treatment of transfected HEK293T cells with 1  $\mu$ M of the degraders for 6 h. We chose compounds **4** and **5** from the pyridazinone series as representative examples of alkyl and PEG linkers. We observed a significant decrease in donor luminescence with both our pyridazinone and TP-238 degraders compared to the untreated DMSO control, indicating degradation of the construct (**Figure 4C**). To validate proteasome dependence, we pre-treated cells with 10  $\mu$ M of proteasome inhibitor MG-132. This pre-treatment resulted in rescue of degradation, with some additional stabilization of the donor signal, supporting a proteasome-dependent mechanism.

As luciferase enzyme-based assays are prone to interference due to potential inhibitors,<sup>33</sup> we were concerned about any off-target effects of our molecules on the Nluc-BPTF construct. To demonstrate that these degraders bind to the BPTF bromodomain and not Nluc, we pre-treated transfected HEK293T cells with the monovalent BPTF inhibitor **19** that we had previously characterized.<sup>12</sup> We tested this in the ternary complex assay format and observed a dose-dependent dissociation of the ternary complex with increasing concentrations of **19** (Figure S4). This further validated that the ternary complex formation is BPTF bromodomain-dependent.

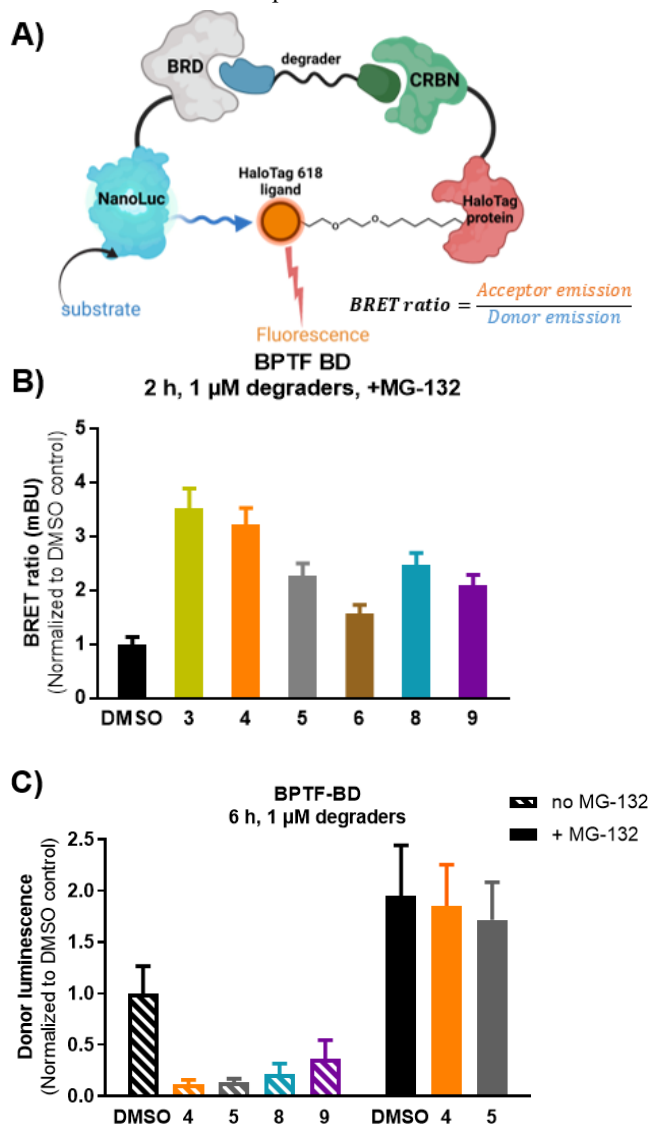


**Figure 4.** A) NanoBRET assay format used to monitor ternary complex formation and degradation in HEK293T cells. B) In-cell ternary complex formation was rank-ordered by determining fold-change in BRET ratio compared to the DMSO control. C) Degradation of the Nluc-BPTF-BD construct was studied by measuring the total donor luminescence in the absence of MG-132. Degradation was rescued on pre-treatment with 10  $\mu\text{M}$  MG-132.

**In-cell ternary complex formation and degradation of full-length BRD9 via NanoBRET.** We further characterized our compounds for ternary complex formation and degradation of

full-length BRD9 using NanoBRET. BRD9 is a reported off-target for the pyridazinone scaffold<sup>12,34</sup> and TP-238.<sup>25</sup> Due to its smaller size (75 kDa) compared to full-length BPTF (~300 kDa), we expected full-length BRD9 (BRD9-FL) to be more amenable to transfection and easier to study in this assay compared to full-length BPTF. We could also use dBRD9<sup>35</sup> as a positive control to validate our assay in this system. We used compounds **4**, **5**, **8** and **9** as examples of alkyl and PEG linker containing degraders. For the pyridazinone degraders, we observed a similar trend to our BPTF ternary complex data, where compound **4** showed a higher BRET signal than **5**, which was comparable in magnitude to dBRD9 (2-fold over DMSO control) (Figure 5A). For the TP-238 series, the BRET ratios were slightly lower than dBRD9 (~1.5-fold over DMSO), which is consistent with the lower affinity of the TP-238 ligand for BRD9, although given the data in Table 1, we expected it to show a much lower signal. It is unclear if the full-length BRD9 shows some additional affinity for this scaffold in the context of this experiment.

We then monitored degradation of the Nluc-BRD9-FL construct under similar conditions as our BPTF study. Encouragingly, both compound **4** and **5** caused degradation of full-length BRD9, comparable to the dBRD9 control (Figure 5B). Consistent with their ternary complex behavior, compounds **8** and **9** also degrade BRD9-FL, albeit not as potently as dBRD9. These studies confirmed that both series of degrader molecules can engage full-length bromodomain-containing proteins in cells and induce their degradation. They also established the robustness of our NanoBRET assay, indicating that it is applicable to multiple bromodomain-containing constructs.

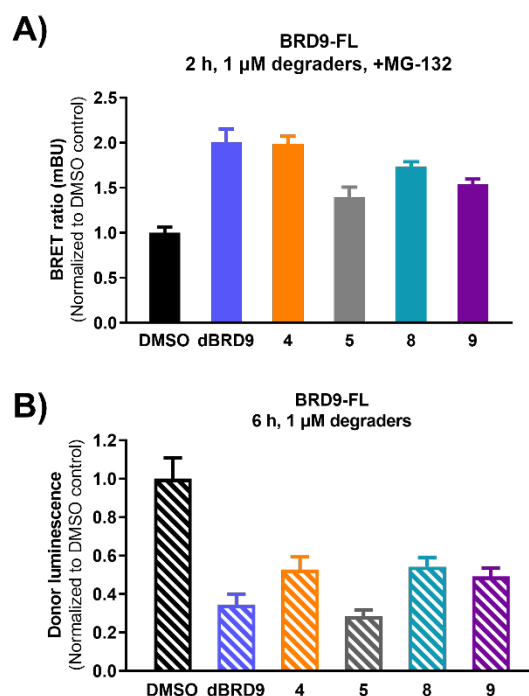


**Figure 5.** In-cell NanoBRET experiments with BRD9-FL, indicating A) ternary complex formation and B) degradation of the Nluc-BRD9-FL fusion.

**Degradation of endogenous BPTF, CECR2, and BRD9.** With well-characterized compounds in hand, we tested their

ability to degrade endogenous BPTF in HEK293T cells. We used the 6 h treatment condition from our NanoBRET assay and monitored the total amount of BPTF in lysates through western blotting. Surprisingly, our pyridazinone degraders did not show degradation of endogenous BPTF or a second class I bromodomain-containing protein, PCAF, or the class IV bromodomain BRD9 under these conditions up to 10  $\mu$ M of the compounds (**Figure S7**). In contrast, the TP-238 series demonstrated a moderate effect with partial degradation between 0.1–1  $\mu$ M concentrations against BPTF, with compound **8** demonstrating the higher potency. (**Figure 6A**). Taken together with our NanoBRET data, we hypothesize that the minimal effect of these compounds on full-length BPTF in endogenous systems may be a cell-line dependent effect and the levels of functional BPTF available for degradation. In cells, endogenous BPTF is a subunit of the NURF complex, which may hinder its accessibility by heterobifunctional degraders. The moderate effect observed via the TP-238 scaffold hints towards longer, pre-organized linkers (such as the piperazine moiety in compounds **8** and **9**) which may be able to improve the activity of BPTF degraders.

Due to the modest effects observed in degrading endogenous BPTF, we sought to examine the main off-target proteins of the two scaffolds. TP-238 is a high affinity inhibitor of CECR2 so we selected compounds **8** and **9** as potential degraders of CECR2 over molecules **4** and **5**. Encouragingly, we observed significant degradation of CECR2 between 0.02–0.63  $\mu$ M (**Figure 6B**) in HEK293T cells after 6 h treatment with compound **8**. A hook-effect was observed at higher concentration. After 12 h, we saw significant degradation at lower pM concentrations (up to 250 pm/0.0025  $\mu$ M), while at certain concentrations protein resynthesis was observed. The appearance of the CECR2 band across all concentrations was observed after 24 hr (**Figure S8**). This effect may result from breakdown of **8** via hydrolysis of the cereblon (CRBN) motif or cleavage of the alkyl linker under physiological conditions. Together these results support the first degraders of the class I bromodomain-containing protein CECR2. These tool compounds are anticipated to enable future mechanistic studies of the functional effects of regulating CECR2 and CERF function and will be optimized in future studies to improve degradation of BPTF.

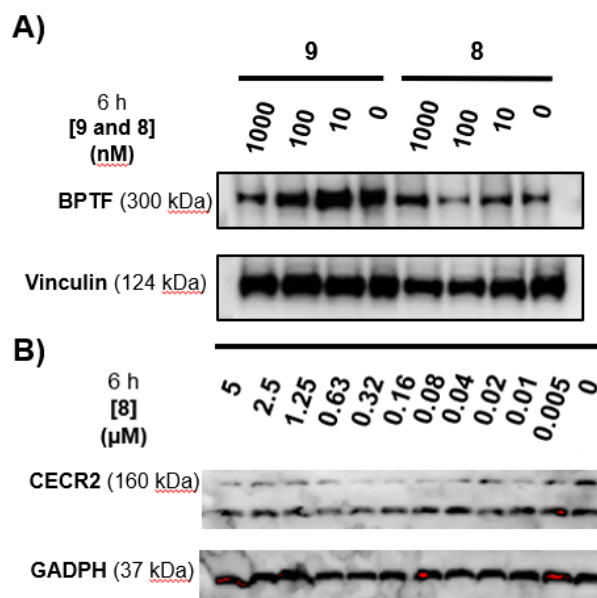


**Figure 6.** Western blotting in HEK293T cells with treatment of **A)** compounds **8** and **9** with BPTF for 6 h and **B)** compound **8** with CECR2 for 6 h.

## CONCLUSIONS

We describe the design of heterobifunctional degraders targeting class I and BRD9 bromodomains, using two different scaffolds with distinct selectivity profiles. We explore exit vectors based on tetrahydroisoquinoline-substituted pyridazinones, evaluating both alkyl and PEG linkers, and a rigid piperazine linker tethered to the TP-238 scaffold. Using an in vitro AlphaScreen assay to assess ternary complex formation, we discover that several of the pyridazinone analogues demonstrate a selectivity bias for BPTF and BRD9 over PCAF and CECR2. For the TP-238 degraders, the piperazine-based linker design is found to be more potent in this ternary complex analysis. We further use an in-cell NanoBRET assay to show that our degraders are cell-permeable and form ternary complexes with nanoluciferase-fused BPTF bromodomain and full-length BRD9 constructs. In the absence of a proteasome inhibitor, these fusion constructs are also degraded when treated with our degrader scaffolds. However, we find that our pyridazinone-based degraders do not show degradation activity for endogenous BPTF. In contrast the TP-238 degraders demonstrate a moderate effect on BPTF levels and a strong dose-dependent attenuation of CECR2 levels via western blotting. In the case of BPTF and CECR2, **8** and **9**, represent the first degraders of either protein. These tool compounds provide a starting point to evaluate the effects of targeted protein degradation in cancer models. These include the recently demonstrated role of CECR2 in breast cancer metastasis<sup>23</sup> and pancreatic cancer driven by high levels of BPTF and MYC.<sup>36</sup> Further optimization of our first-generation degraders and a more extensive study of various model cell lines will be evaluated for targeting these important nucleosome remodeling complexes.

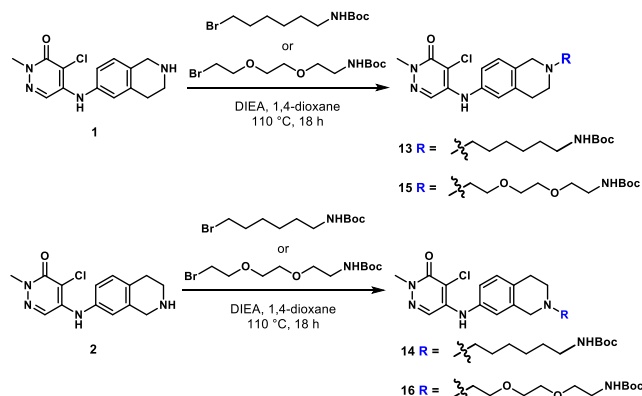
## EXPERIMENTAL SECTION

**Materials and Methods.** All commercially available reagents were used without further purification. Flash column chromatography was performed on a Teledyne-Isco Rf-plus

CombiFlash instrument with RediSep columns. NMR spectra were collected on a Bruker Avance III AX-400 or a Bruker Avance III HD-500 equipped with a Prodigy TCI cryoprobe. Chemical shifts ( $\delta$ ) were reported in parts per million (ppm) and referenced to residual solvent signals for Chloroform-*d* ( $^1\text{H}$  7.26 ppm), Dimethyl Sulfoxide-*d*<sub>6</sub> ( $^1\text{H}$  2.50 ppm,  $^{13}\text{C}$  39.5 ppm) and Methanol-*d*<sub>4</sub> ( $^1\text{H}$  3.31 ppm,  $^{13}\text{C}$  49.0 ppm). Coupling constants (*J*) are in Hz. Splitting patterns were reported as s (singlet), d (doublet), t (triplet), q (quartet) and m (multiplet). High resolution ESI-MS spectra were recorded on a Thermo Fischer Orbitrap Velos equipped with an autosampler. Where stated, compounds were purified by reverse-phase high-performance liquid chromatography (RP-HPLC) on a C-18 column using 0.1% TFA water and CH<sub>3</sub>CN as solvents and TFA salts were quantified using the procedure described by Carlson et al.<sup>37</sup>

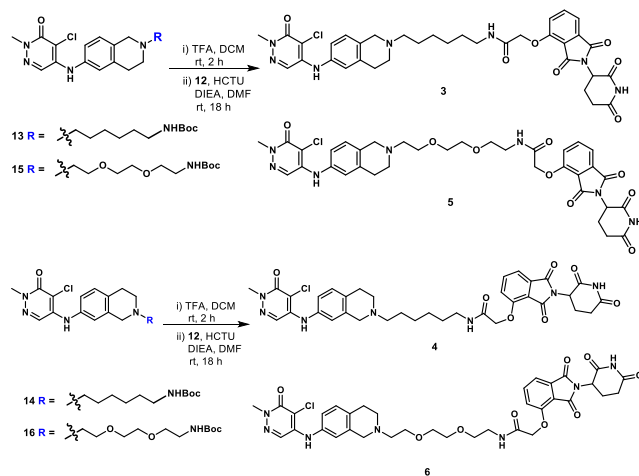
**Purity Analysis.** All compounds tested in cells were  $\geq 95\%$  pure by RP-HPLC. Compounds **3-6** and **8-10** were run on a RP-HPLC with a C-18 column. A gradient of 0-40% ACN in 0.1% TFA H<sub>2</sub>O over 60 min was used for compounds **3**, **5** and **6**, and 0-60% ACN in 0.1% TFA H<sub>2</sub>O over 60 min for compounds **4**, **8**, **9** and **10**. Spectral traces are shown in **Figure S9**.

**Synthetic methods.** The synthesis and characterization of compounds **1** and **2** were described previously.<sup>12</sup> TP-238 (**7**) was purchased from Cayman Chemical.



**Scheme 1.** Synthesis of intermediates **13-16**.

**General procedure A for the synthesis of intermediates 13-16.** Compound **1** or **2** (1.0 eq.) was stirred in 1,4-dioxane at room temperature, followed by addition of the N-Boc linker (1.1 eq.) and *N,N*-Diisopropylethylamine (1.5 eq.). The reaction mixture was heated in a sealed tube at 110 °C for 18 h. Following completion of the reaction, the 1,4-dioxane was removed by rotary evaporation. The crude mixture was extracted into ethyl acetate, washed with a saturated sodium bicarbonate solution (3×20 mL) and finally with brine (20 mL). The organic layer was dried over magnesium sulfate, filtered, concentrated in vacuo and purified by flash column chromatography (CombiFlash Rf system: 4 g silica, DCM/methanol, 0-20% methanol, 30 minutes).

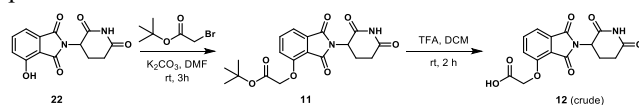


**Scheme 2:** Synthesis of compounds **3-6**.

**General procedure B for the synthesis of compounds 3-6.**

**Step 1:** Compounds **13-16** were stirred in DCM at room temperature, followed by addition of trifluoroacetic acid (5.0 eq.) and stirred at room temperature for an additional 2 h. Following completion of the reaction, the mixture was blown dry under a stream of nitrogen and the crude product was used without further purification.

**Step 2:** The crude product from Step 1 (1.0 eq.) was stirred in dry DMF and DIEA (4.0 eq.) at room temperature. A mixture of **12** (1.2 eq.) and HCTU (1.2 eq.) in dry DMF was then added and the reaction mixture was stirred at room temperature for 16 h. A portion of the crude material was then purified by reverse-phase HPLC.



**Scheme 3.** Synthesis of 2-((2-(2,6-dioxopiperidin-3-yl)-1,3-dioxoisindolin-4-yl)oxy)acetic acid (**12**).

**tert-butyl 2-((2-(2,6-dioxopiperidin-3-yl)-1,3-dioxoisindolin-4-yl)oxy)acetate (**11**).** Compound **11** was synthesized according to literature procedures.<sup>38</sup> 2-(2,6-dioxopiperidin-3-yl)-4-hydroxyisindoline-1,3-dione (**22**) (240 mg, 0.88 mmol, 1.0 eq.) was dissolved in DMF (2 mL) at room temperature, followed by the addition of potassium carbonate (180 mg, 1.30 mmol, 1.5 eq.) and *tert*-butyl 2-bromoacetate (186 mg, 0.95 mmol, 1.1 eq.). The reaction mixture was stirred at room temperature. After 2 h, the mixture was extracted into ethyl acetate, washed with water (20 mL) and finally with brine (20 mL). The organic layer was dried over magnesium sulfate, filtered, concentrated in vacuo and purified by flash column chromatography (CombiFlash Rf system: 24 g silica, hexanes/ethyl acetate, 0-100% ethyl acetate, 16 minutes) to obtain a white solid (198 mg, 58% yield).  $^1\text{H}$  NMR (500 MHz, DMSO)  $\delta$  11.11 (s, 1H), 7.80 (dd, *J* = 8.5, 7.2 Hz, 1H), 7.48 (d, *J* = 6.9 Hz, 1H), 7.38 (d, *J* = 8.1 Hz, 1H), 5.10 (dd, *J* = 12.8, 5.5 Hz, 1H), 4.97 (s, 2H), 2.89 (ddd, *J* = 16.9, 13.8, 5.5 Hz, 1H), 2.63–2.56 (m, 1H), 2.55–2.51 (m, 1H), 2.09–2.00 (m, 1H), 1.43 (s, 9H), H<sub>2</sub>O from solvent at 3.32 ppm, ethyl acetate impurity at 4.02 ppm, 1.99 ppm and 1.17 ppm (4.8% by weight).



**2-((2-(2,6-dioxopiperidin-3-yl)-1,3-dioxoisindolin-4-yl)oxy)acetic acid (12).** Compound **11** was stirred in DCM at room temperature, followed by addition of trifluoroacetic acid (5.0 eq.) and stirred at room temperature for an additional 2 h. Following completion of the reaction, the mixture was blown dry under a stream of nitrogen and the crude product **12** was used without further purification.

**tert-butyl (5-(6-((5-chloro-1-methyl-6-oxo-1,6-dihydropyridazin-4-yl)amino)-3,4-dihydroisoquinolin-2(1H)-yl)pentyl)carbamate (13).** Following the general procedure A, (1 (63 mg, 0.22 mmol, 1.0 eq.), tert-butyl (6-bromoethyl)carbamate (67 mg, 0.24 mmol, 1.1 eq.), *N,N*-Diisopropylethylamine (57  $\mu$ L, 0.33 mmol, 1.5 eq.), 1,4-dioxane (1 mL)), product **13** was obtained as a brown solid (42 mg, 40% yield). <sup>1</sup>H NMR (500 MHz, DMSO)  $\delta$  8.61 (s, 1H), 7.61 (s, 1H), 7.08 (d, *J* = 8.1 Hz, 1H), 6.99 (dd, *J* = 8.1, 2.3 Hz, 1H), 6.97 (d, *J* = 2.2 Hz, 1H), 6.76 (t, *J* = 5.8 Hz, 1H), 3.60 (s, 3H), 3.51 (s, 2H), 2.89 (q, *J* = 6.6 Hz, 2H), 2.79 (t, *J* = 5.9 Hz, 2H), 2.62 (t, *J* = 5.9 Hz, 2H), 2.42 (t, *J* = 7.3 Hz, 2H), 1.50 (q, *J* = 7.2 Hz, 2H), 1.37 (s, 9H), 1.33 – 1.21 (m, 4H), H<sub>2</sub>O from solvent at 3.32 ppm, DCM impurity at 5.76 ppm (2.5% by weight). <sup>13</sup>C NMR (126 MHz, DMSO)  $\delta$  157.0, 155.6, 142.6, 136.1, 135.5, 132.1, 127.5, 127.3, 123.6, 121.3, 107.8, 77.3, 57.7, 55.2, 50.4, 29.5, 28.3, 26.6, 26.5, 26.2 (one resonance obscured by solvent, two resonances overlapping). HRMS (ESI-TOF) calculated for C<sub>25</sub>H<sub>37</sub>ClN<sub>5</sub>O<sub>3</sub><sup>+</sup> [M+H]<sup>+</sup>: 490.2579, observed 490.2546.

**tert-butyl (6-(7-((5-chloro-1-methyl-6-oxo-1,6-dihydropyridazin-4-yl)amino)-3,4-dihydroisoquinolin-2(1H)-yl)hexyl)carbamate (14).** Following the general procedure A, (2 (60 mg, 0.21 mmol, 1.0 eq.), tert-butyl (6-bromoethyl)carbamate (64 mg, 0.23 mmol, 1.1 eq.), *N,N*-Diisopropylethylamine (54  $\mu$ L, 0.31 mmol, 1.5 eq.), 1,4-dioxane (1 mL)), product **14** was obtained as a yellow solid (28 mg, 26% yield). <sup>1</sup>H NMR (500 MHz, DMSO)  $\delta$  8.61 (s, 1H), 7.60 (s, 1H), 7.11 (d, *J* = 8.1 Hz, 1H), 7.00 (dd, *J* = 8.1, 2.3 Hz, 1H), 6.93 (d, *J* = 2.3 Hz, 1H), 6.75 (t, *J* = 5.8 Hz, 1H), 3.60 (s, 3H), 3.51 (s, 2H), 2.89 (q, *J* = 6.6 Hz, 2H), 2.78 (t, *J* = 5.9 Hz, 2H), 2.63 (t, *J* = 5.8 Hz, 2H), 2.41 (t, *J* = 7.3 Hz, 2H), 1.50 (t, *J* = 7.2 Hz, 2H), 1.36 (s, 9H), 1.27 (m, 4H), H<sub>2</sub>O from solvent at 3.32 ppm. <sup>13</sup>C NMR (126 MHz, DMSO)  $\delta$  157.0, 155.6, 142.6, 136.2, 135.7, 131.4, 129.3, 127.5, 121.9, 121.7, 107.7, 77.3, 57.6, 55.4, 50.5, 29.5, 28.3, 26.6, 26.5, 26.2 (one resonance obscured by solvent, two resonances overlapping). HRMS (ESI-TOF) calculated for C<sub>25</sub>H<sub>37</sub>ClN<sub>5</sub>O<sub>3</sub><sup>+</sup> [M+H]<sup>+</sup>: 490.2579, observed 490.2547.

**tert-butyl (2-(2-(2-(6-((5-chloro-1-methyl-6-oxo-1,6-dihydropyridazin-4-yl)amino)-3,4-dihydroisoquinolin-2(1H)-yl)ethoxy)ethoxy)ethyl)carbamate (15).** Following the general procedure A, (1 (60 mg, 0.21 mmol, 1.0 eq.), tert-butyl (2-(2-(2-bromoethoxy)ethoxy)ethyl)carbamate (71 mg, 0.23 mmol, 1.1 eq.), *N,N*-Diisopropylethylamine (54  $\mu$ L, 0.31 mmol, 1.5 eq.), 1,4-dioxane (1 mL)), product **15** was obtained as a brown solid (53 mg, 49% yield). <sup>1</sup>H NMR (500 MHz, DMSO)  $\delta$  8.62 (s, 1H), 7.60 (s, 1H), 7.06 (d, *J* = 8.1 Hz, 1H), 6.99 (dd, *J* = 8.1, 2.3 Hz, 1H), 6.97 (d, *J* = 2.1 Hz, 1H), 6.75 (t, *J* = 5.8 Hz, 1H), 3.61 – 3.58 (m, 7H, overlapping resonances), 2.73 – 2.68 (m, 4H), 3.38 (t, *J* = 6.2 Hz, 2H), 3.06 (q, *J* = 6.1 Hz, 2H), 2.79 (t, *J* = 5.9 Hz, 2H), 2.70 (t, *J* = 5.8 Hz, 2H), 2.64 (t, *J* = 5.9 Hz, 2H), 1.37 (s, 9H), H<sub>2</sub>O from solvent at 3.32 ppm. <sup>13</sup>C NMR (126 MHz, DMSO)  $\delta$  157.0, 155.6, 142.6, 136.1, 135.3, 132.1, 127.5, 127.3, 123.6, 121.4, 107.8, 77.6, 69.7, 69.5, 69.2, 68.5,

57.0, 55.4, 50.7, 28.7, 28.2 (one resonance obscured by solvent, two resonances overlapping). HRMS (ESI-TOF) calculated for C<sub>25</sub>H<sub>37</sub>ClN<sub>5</sub>O<sub>5</sub><sup>+</sup> [M+H]<sup>+</sup>: 522.2478, observed 522.2444.

**tert-butyl (2-(2-(2-(7-((5-chloro-1-methyl-6-oxo-1,6-dihydropyridazin-4-yl)amino)-3,4-dihydroisoquinolin-2(1H)-yl)ethoxy)ethoxy)ethyl)carbamate (16).** Following the general procedure A, (2 (75 mg, 0.26 mmol, 1.0 eq.), tert-butyl (2-(2-(2-bromoethoxy)ethoxy)ethyl)carbamate (89 mg, 0.28 mmol, 1.1 eq.), *N,N*-Diisopropylethylamine (67  $\mu$ L, 1.5 mmol, 1.5 eq.), 1,4-dioxane (1 mL)), product **16** was obtained as a brown solid (39 mg, 36% yield). <sup>1</sup>H NMR (500 MHz, DMSO)  $\delta$  8.61 (s, 1H), 7.60 (s, 1H), 7.11 (d, *J* = 8.2 Hz, 1H), 7.00 (dd, *J* = 8.1, 2.3 Hz, 1H), 6.92 (d, *J* = 2.3 Hz, 1H), 6.74 (t, *J* = 5.8 Hz, 1H), 3.63 – 3.56 (m, 7H, overlapping resonances), 3.53 – 3.49 (m, 4H), 3.38 (t, *J* = 6.1 Hz, 2H), 3.05 (q, *J* = 6.0 Hz, 2H), 2.78 (t, *J* = 5.7 Hz, 2H), 2.71 (t, *J* = 5.8 Hz, 2H), 2.64 (t, *J* = 5.9 Hz, 2H), 1.36 (s, 9H), H<sub>2</sub>O from solvent at 3.32 ppm, DCM impurity at 5.75 ppm (2.4% by weight). <sup>13</sup>C NMR (126 MHz, DMSO)  $\delta$  157.0, 155.6, 142.6, 136.1, 135.7, 131.2, 129.3, 127.5, 121.9, 121.7, 107.7, 77.6, 69.7, 69.5, 69.2, 68.5, 56.9, 55.6, 50.8, 28.2 (overlapping resonances), (one resonance obscured by solvent, two resonances overlapping). HRMS (ESI-TOF) calculated for C<sub>25</sub>H<sub>37</sub>ClN<sub>5</sub>O<sub>5</sub><sup>+</sup> [M+H]<sup>+</sup>: 522.2478, observed 522.2442.

**N-(5-(6-((5-chloro-1-methyl-6-oxo-1,6-dihydropyridazin-4-yl)amino)-3,4-dihydroisoquinolin-2(1H)-yl)pentyl)-2-((2-(2,6-dioxopiperidin-3-yl)-1,3-dioxoisindolin-4-yl)oxy)acetamide (3).** Following the general procedure B, compound **13** was Boc deprotected in Step 1 and the crude material was used for Step 2: (29 mg, 0.07 mmol, 1.0 eq.), **11** (30 mg, 0.09 mmol, 1.2 eq.), HCTU (37 mg, 0.09 mmol, 1.2 eq.), *N,N*-Diisopropylethylamine (52  $\mu$ L, 0.30 mmol, 4.0 eq.), DMF (0.5 mL). A portion of the crude product was purified by reverse-phase semi-prep HPLC (5-30% ACN in 0.1% TFA water over 25 minutes, C18 column) to obtain product **3** as a white solid (2X TFA salt). <sup>1</sup>H NMR (500 MHz, DMSO)  $\delta$  11.12 (s, 1H), 9.76 (s, 1H), 8.79 (s, 1H), 8.02 – 7.92 (m, 1H), 7.82 (dd, *J* = 8.5, 7.3 Hz, 1H), 7.66 (s, 1H), 7.51 (d, *J* = 7.2 Hz, 1H), 7.41 (d, *J* = 8.5 Hz, 1H), 7.23 (d, *J* = 8.3 Hz, 1H), 7.16 (dd, *J* = 8.3, 2.3 Hz, 1H), 7.13 (d, *J* = 2.2 Hz, 1H), 5.12 (dd, *J* = 12.9, 5.4 Hz, 1H), 4.78 (s, 2H), 4.57 – 4.51 (m, 1H), 4.26 (dd, *J* = 15.5, 8.1 Hz, 1H), 3.75 – 3.67 (m, 1H), 3.62 (s, 3H), 3.36 – 3.24 (m, 1H), 3.24 – 3.13 (m, 4H), 3.13 – 2.97 (m, 2H), 2.95 – 2.81 (m, 1H), 2.65 – 2.56 (m, 1H), 2.54 (d, *J* = 4.4 Hz, 1H), 2.09 – 1.99 (m, 1H), 1.78 – 1.67 (m, 2H), 1.58 – 1.43 (m, 2H), 1.39 – 1.27 (m, 4H). <sup>13</sup>C NMR (126 MHz, DMSO)  $\delta$  172.8, 169.9, 166.7, 165.5, 157.0, 155.0, 142.0, 138.1, 136.9, 133.0, 132.5, 127.7, 124.7, 122.6, 121.8, 120.4, 116.8, 116.1, 109.2, 67.7, 55.1, 51.8, 48.8, 38.1, 30.9, 28.8, 25.7, 25.6, 25.0, 23.4, 22.0 (one resonance obscured by solvent, three resonances overlapping). HRMS (ESI-TOF) calculated for C<sub>35</sub>H<sub>39</sub>ClN<sub>7</sub>O<sub>7</sub><sup>+</sup> [M+H]<sup>+</sup>: 704.2594, observed 704.2552.

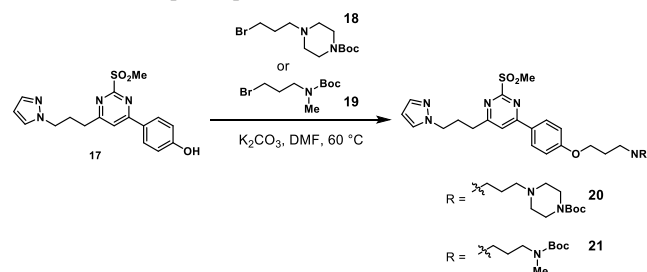
**N-(6-(7-((5-chloro-1-methyl-6-oxo-1,6-dihydropyridazin-4-yl)amino)-3,4-dihydroisoquinolin-2(1H)-yl)hexyl)-2-((2-(2,6-dioxopiperidin-3-yl)-1,3-dioxoisindolin-4-yl)oxy)acetamide (4).** Following the general procedure B, compound **14** was boc deprotected in Step 1 and the crude material was used for Step 2: (13 mg, 0.03 mmol, 1.0 eq.), **11** (13 mg, 0.04 mmol, 1.2 eq.), HCTU (17 mg, 0.04 mmol, 1.2 eq.), *N,N*-Diisopropylethylamine (23  $\mu$ L, 0.13 mmol, 4.0 eq.), DMF (0.5 mL). A

portion of the crude product was purified by reverse-phase semi-prep HPLC (5-40% ACN in 0.1% TFA water over 25 minutes, C18 column) to obtain product **4** as a white solid (2X TFA salt). <sup>1</sup>H NMR (500 MHz, DMSO) δ 11.12 (s, 1H), 9.84 (s, 1H), 8.79 (s, 1H), 7.97 (t, *J* = 5.5 Hz, 1H), 7.82 (dd, *J* = 8.5, 7.3 Hz, 1H), 7.64 (s, 1H), 7.51 (d, *J* = 7.2 Hz, 1H), 7.40 (d, *J* = 8.5 Hz, 1H), 7.28 (d, *J* = 8.3 Hz, 1H), 7.18 (dd, *J* = 8.2, 2.3 Hz, 1H), 7.08 (d, *J* = 2.3 Hz, 1H), 5.12 (dd, *J* = 12.9, 5.4 Hz, 1H), 4.78 (s, 2H), 4.63 – 4.49 (m, 1H), 4.27 (dd, *J* = 15.7, 8.0 Hz, 1H), 3.72 (d, *J* = 12.4 Hz, 1H), 3.62 (s, 3H), 3.35 – 3.25 (m, 1H), 3.24 – 3.12 (m, 4H), 3.12 – 2.99 (m, 1H), 2.96 – 2.83 (m, 1H), 2.68 – 2.55 (m, 1H), 2.54 (d, *J* = 4.5 Hz, 0H), 2.10 – 1.95 (m, 1H), 1.81 – 1.66 (m, 2H), 1.55 – 1.40 (m, 2H), 1.36 – 1.22 (m, 4H). <sup>13</sup>C NMR (126 MHz, DMSO) δ 172.8, 169.9, 166.7, 166.7, 165.5, 158.1, 157.0, 155.0, 142.1, 137.1, 136.9, 133.0, 129.6, 129.5, 127.7, 123.1, 120.9, 120.4, 116.8, 116.1, 109.0, 67.7, 55.1, 51.8, 49.0, 48.8, 38.1, 30.9, 28.8, 25.8, 25.6, 24.5, 23.4, 22.0 (one resonance obscured by solvent). HRMS (ESI-TOF) calculated for C<sub>35</sub>H<sub>38</sub>ClN<sub>7</sub>O<sub>9</sub><sup>+</sup> [M+H]<sup>+</sup>: 735.2420, observed 704.2554.

**N-(2-(2-(2-(6-((5-chloro-1-methyl-6-oxo-1,6-dihydropyridazin-4-yl)amino)-3,4-dihydroisoquinolin-2(1H-yl)ethoxy)ethoxy)ethyl)-2-((2-(2,6-dioxopiperidin-3-yl)-1,3-dioxoisindolin-4-yl)oxy)acetamide (5).** Following the general procedure B, compound **15** was Boc deprotected in Step 1 and the crude material was used for Step 2: (27 mg, 0.06 mmol, 1.0 eq.), **11** (25 mg, 0.08 mmol, 1.2 eq.), HCTU (32 mg, 0.08 mmol, 1.2 eq.), *N,N*-Diisopropylethylamine (45 μL, 0.26 mmol, 4.0 eq.), DMF (0.5 mL). A portion of the crude product was purified by reverse-phase semi-prep HPLC (5-30% ACN in 0.1% TFA water over 25 minutes, C18 column) to obtain product **5** as a white solid (1X TFA salt). <sup>1</sup>H NMR (500 MHz, DMSO) δ 11.13 (s, 1H), 10.10 (s, 1H), 8.77 (s, 1H), 8.00 (t, *J* = 5.7 Hz, 1H), 7.81 (dd, *J* = 8.5, 7.3 Hz, 1H), 7.65 (s, 1H), 7.50 (d, *J* = 7.2 Hz, 1H), 7.41 (d, *J* = 8.6 Hz, 1H), 7.21 (d, *J* = 8.3 Hz, 1H), 7.14 (dd, *J* = 8.3, 2.2 Hz, 1H), 7.11 (d, *J* = 2.2 Hz, 1H), 5.11 (dd, *J* = 12.9, 5.4 Hz, 1H), 4.79 (s, 2H), 4.53 (d, *J* = 15.4 Hz, 1H), 4.34 (dd, *J* = 15.6, 7.3 Hz, 1H), 3.84 (t, *J* = 5.0 Hz, 2H), 3.77 – 3.70 (m, 1H), 3.64 – 3.62 (m, 2H), 3.61 (s, 3H), 3.61 – 3.58 (m, 2H), 3.50 (t, *J* = 5.8 Hz, 2H), 3.46 – 3.37 (m, 3H), 3.34 (q, *J* = 5.8 Hz, 2H), 3.20 – 3.09 (m, 1H), 3.09 – 2.99 (m, 1H), 2.95 – 2.84 (m, 1H), 2.60 (s, 1H), 2.57 – 2.52 (m, 1H), 2.08 – 1.99 (m, 1H). <sup>13</sup>C NMR (126 MHz, DMSO) δ 172.8, 169.9, 166.9, 166.7, 165.5, 157.0, 154.9, 142.0, 138.1, 137.0, 133.0, 132.4, 127.7, 127.7, 124.5, 122.6, 121.7, 120.4, 116.8, 116.1, 109.2, 69.6, 69.4, 68.8, 67.5, 64.4, 54.3, 52.1, 49.0, 48.8, 38.4, 30.9, 24.7, 22.0 (one resonance obscured by solvent). HRMS (ESI-TOF) calculated for C<sub>35</sub>H<sub>39</sub>ClN<sub>7</sub>O<sub>9</sub><sup>+</sup> [M+H]<sup>+</sup>: 736.2492, observed 736.2445.

**N-(2-(2-(2-(7-((5-chloro-1-methyl-6-oxo-1,6-dihydropyridazin-4-yl)amino)-3,4-dihydroisoquinolin-2(1H-yl)ethoxy)ethoxy)ethyl)-2-((2-(2,6-dioxopiperidin-3-yl)-1,3-dioxoisindolin-4-yl)oxy)acetamide (6).** Following the general procedure B, compound **16** was Boc deprotected in Step 1 and the crude material was used for Step 2: (27 mg, 0.06 mmol, 1.0 eq.), **11** (26 mg, 0.08 mmol, 1.2 eq.), HCTU (32 mg, 0.08 mmol, 1.2 eq.), *N,N*-Diisopropylethylamine (45 μL, 0.26 mmol, 4.0 eq.), DMF (0.5 mL). A portion of the crude product was purified by reverse-phase semi-prep HPLC (5-30% ACN in 0.1% TFA water over 25 minutes, C18 column) to obtain

product **6** as a white solid (2X TFA salt). <sup>1</sup>H NMR (500 MHz, DMSO) δ 11.13 (s, 1H), 9.99 (s, 1H), 7.97 (q, *J* = 5.7 Hz, 1H), 7.81 (dd, *J* = 8.5, 7.3 Hz, 1H), 7.62 (s, 1H), 7.50 (d, *J* = 7.2 Hz, 1H), 7.40 (d, *J* = 8.5 Hz, 1H), 7.26 (d, *J* = 8.3 Hz, 1H), 7.17 (dd, *J* = 8.2, 2.3 Hz, 1H), 7.08 (d, *J* = 2.3 Hz, 1H), 5.11 (dd, *J* = 12.9, 5.4 Hz, 1H), 4.77 (s, 2H), 4.53 (d, *J* = 15.7 Hz, 1H), 4.40 – 4.31 (m, 1H), 3.82 (t, *J* = 5.0 Hz, 2H), 3.79 – 3.71 (m, 1H), 3.67 – 3.55 (m, 7H), 3.48 (t, *J* = 5.8 Hz, 2H), 3.45 – 3.36 (m, 3H), 3.33 (q, *J* = 5.5 Hz, 2H), 3.18 – 3.08 (m, 1H), 3.08 – 2.99 (m, 1H), 2.95 – 2.84 (m, 1H), 2.64 – 2.56 (m, 1H), 2.57 – 2.52 (m, 1H), 2.08 – 1.99 (m, 1H). <sup>13</sup>C NMR (126 MHz, DMSO) δ 172.8, 169.9, 166.9, 166.7, 165.5, 157.0, 154.9, 142.1, 137.1, 137.0, 133.0, 129.6, 129.3, 127.6, 123.1, 121.0, 120.3, 116.7, 116.1, 108.9, 69.6, 69.3, 68.8, 67.5, 64.4, 54.4, 52.2, 49.3, 48.8, 38.3, 30.9, 24.3, 22.0 (one resonance obscured by solvent, two resonances overlapping). HRMS (ESI-TOF) calculated for C<sub>35</sub>H<sub>39</sub>ClN<sub>7</sub>O<sub>9</sub><sup>+</sup> [M+H]<sup>+</sup>: 736.2492, observed 736.2447.



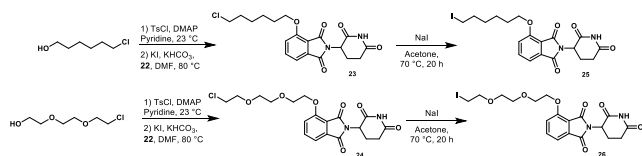
**Scheme 4. Synthesis of Intermediates 20 and 21**

**General Procedure C for the synthesis intermediates 20 and 21.** To a mixture of the sulfone **17**<sup>39</sup> (1.0 eq) in DMF (0.1 M) was added the bromide **18** or **19** (2.0 eq) and K<sub>2</sub>CO<sub>3</sub> (2.0 eq). The resulting mixture was heated to reflux and stirred. Upon completion, ethyl acetate and water were added. The layers were separated, and the organic layer was washed sequentially with water (2x), 10% aq LiCl, and brine. The organic layer was dried over MgSO<sub>4</sub> and the volatiles were removed via rotary evaporation. The resulting residue was purified by column chromatography (CombiFlash Rf system: 24 g silica, hexanes/ethyl acetate, 0-100% ethyl acetate, 16 mins).

**Tert-butyl 4-(3-(4-(6-(3-(1H-pyrazol-1-yl)propyl)-2-(methylsulfonyl)pyrimidin-4-yl)phenoxy)propyl)piperazine-1-carboxylate (20).** Following the general procedure C, sulfone **17** was alkylated with bromide **18**, Sulfone **17**<sup>39</sup> (309 mg, 0.828 mmol, 1.0 eq), bromide **18**<sup>40</sup> (510 mg, 1.66 mmol, 2.0 eq), K<sub>2</sub>CO<sub>3</sub> (229 mg, 1.66 mmol, 2.0 eq), DMF (8.0 mL). Product **20** was obtained as a white solid (445 mg, 90 % yield). <sup>1</sup>H NMR (400 MHz, CDCl<sub>3</sub>) δ 7.96 (d, *J* = 8.5 Hz, 2H), 7.56 (d, *J* = 2.3 Hz, 1H), 7.42 (d, *J* = 2.3 Hz, 1H), 6.96 (d, *J* = 8.5 Hz, 2H), 6.69 (s, 1H), 6.28 (s, 1H), 5.94 (br. s, 1H), 4.27 (t, *J* = 6.3 Hz, 2H), 4.09 (t, *J* = 6.3 Hz, 2H), 3.46–3.41 (m, 6H), 3.34 (s, 3H), 2.54 (t, *J* = 7.3 Hz, 2H), 2.42 (t, *J* = 5.1 Hz, 4H), 2.22–2.14 (m, 2 H), 1.97 (t, *J* = 6.9 Hz, 2H), 1.44 (s, 9H). <sup>13</sup>C (100 MHz, CDCl<sub>3</sub>) δ 165.9, 163.9, 161.7, 154.9, 139.7, 129.7, 128.8, 128.3, 114.8, 106.1, 79.8, 68.0, 66.4, 60.5, 55.2, 53.2, 38.9, 29.7, 28.6, 26.8, 14.3; HRMS (ESI-TOF) calculated for C<sub>30</sub>H<sub>41</sub>N<sub>5</sub>O<sub>5</sub>S<sup>+</sup> [M+H]<sup>+</sup>: 585.2854, observed 584.2836.

**Tert-butyl 3-(4-(6-(3-(1H-pyrazol-1-yl)propyl)-2-(methylsulfonyl)pyrimidin-4-yl)phenoxy)propyl(methyl)carbamate (21).** Following the general procedure C, sulfone **17** was alkylated with bromide **19**<sup>41</sup> (258 mg, 1.03 mmol, 1.5 eq), K<sub>2</sub>CO<sub>3</sub> (227

mg, 1.64 mmol, 1.5 eq), DMF (8.0 mL). Product **21** was obtained as a white solid (275 mg, 65% yield). <sup>1</sup>H NMR (400 MHz, CDCl<sub>3</sub>) δ 7.90 (d, *J* = 8.5 Hz, 2H), 7.51 (d, *J* = 2.3 Hz, 1H), 7.40 (d, *J* = 2.3 Hz, 1H), 6.90 (d, *J* = 8.5 Hz, 2H), 6.69 (s, 1H), 6.27 (br. s, 1H), 6.24 (s, 1H), 4.23 (t, *J* = 6.3 Hz, 2H), 4.00 (t, *J* = 6.3 Hz, 2H), 3.45–3.40 (m, 4H), 3.32 (s, 3H), 2.86 (s, 3H), 2.14 (t, *J* = 6.5 Hz, 2H), 2.00 (t, *J* = 6.5 Hz, 2H), 1.42 (s, 9H); <sup>13</sup>C NMR (100 MHz, CDCl<sub>3</sub>) δ 165.7, 163.9, 161.4, 155.9, 139.5, 129.7, 128.7, 128.2, 114.6, 105.9, 79.5, 65.8, 65.3, 49.3, 45.9, 38.9, 34.6, 29.6, 28.5, 27.8; HRMS (ESI-TOF) calculated for C<sub>26</sub>H<sub>35</sub>N<sub>5</sub>O<sub>5</sub>S<sup>+</sup> [M+H]<sup>+</sup>: 530.2432, observed 530.2435.



**Scheme 5. Synthesis of Intermediates 23–26.**

#### General Procedure D for the synthesis of intermediates 23 and 24.

**Step 1:** To a solution of 6-chlorohexan-1-ol or 2-(2-(2-chloroethoxy)ethoxy)ethan-1-ol (1.0 eq) in pyridine (2.0 M) was added TsCl (1.1 eq) and DMAP (0.1 eq) at 0 °C. The resulting mixture was allowed to warm to 23 °C and stirred for 2 h. Upon completion, EtOAc and H<sub>2</sub>O were added, and the layers were separated. The organic layer was washed sequentially with 1 M aq HCl, H<sub>2</sub>O, and sat. aq. NaHCO<sub>3</sub>, then dried over MgSO<sub>4</sub>. The volatiles were removed via rotary evaporation.

**Step 2:** The resulting crude residues were dissolved in DMF (0.15 M) followed by addition of 2-(2,6-dioxopiperidin-3-yl)-4-hydroxyisoindoline-1,3-dione (**22**) (1.0 eq), KHCO<sub>3</sub> (1.6 eq), KI (0.1 eq). The resulting mixture was heated to 80 °C and stirred for 22 h. Upon completion, ethyl acetate and water were added, and the layers were separated. The organic layer was washed sequentially with 10% aq LiCl, water, and brine, then dried over MgSO<sub>4</sub>. Volatiles were removed via rotary evaporation and the resulting residues were purified via column chromatography (CombiFlash Rf system: 24 g silica, hexanes/ethyl acetate, 0–100% ethyl acetate, 16 mins).

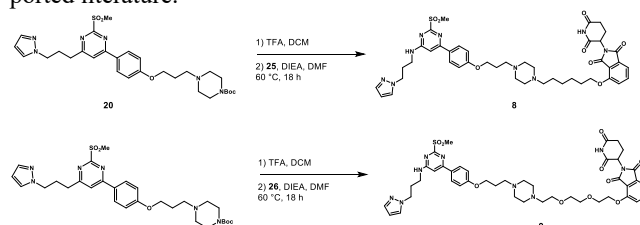
**4-((6-chlorohexyl)oxy)-2-(2,6-dioxopiperidin-3-yl)isoindoline-1,3-dione (**23**)** Following general procedure D, tosylation was performed with 6-chlorohexan-1-ol (1.00 g, 7.35 mmol, 1.0 eq), TsCl (1.54 g, 8.08 mmol, 1.1 eq), DMAP (90.0 mg, 0.735 mmol, 0.1 eq) in Pyridine (3.5 mL). Product was obtained as a white solid and was taken on crude to the next step. Continuing with general procedure D, crude Tosylate (assumed 3.21 mmol, 1.1 eq), 2-(2,6-dioxopiperidin-3-yl)-4-hydroxyisoindoline-1,3-dione (**22**) (800 mg, 2.92 mmol, 1.0 eq), KHCO<sub>3</sub> (468 mg, 4.67 mmol, 1.6 eq), KI (48.2 mg, 0.292 mmol, 0.1 eq) in DMF (20 mL). Product (**23**) was obtained as a yellow solid (337 mg, 29% yield). Note that minor impurities were observed to Cl/I exchange. <sup>1</sup>H NMR (400 MHz, DMSO-*d*<sub>6</sub>) δ 11.1 (br. s, 1H), 7.80 (t, *J* = 7.6 Hz, 1H), 7.51 (d, *J* = 7.3 Hz, 1H), 7.44 (d, *J* = 8.2 Hz, 1H), 5.08 (dd, *J* = 12.3, 5.4 Hz, 1H), 4.21 (t, *J* = 6.4 Hz, 2H), 3.64 (t, *J* = 6.6 Hz, 2H), 2.95 – 2.82 (m, 1H), 2.63 – 2.50 (m, 2H), 2.17 – 1.95 (m, 1H), 1.81–1.69 (m, 4H), 1.53 – 1.37 (m, 4H). <sup>13</sup>C NMR (100 MHz, DMSO-*d*<sub>6</sub>) δ 172.8, 169.9, 166.8, 165.3, 162.1, 156.0, 137.0, 133.2, 119.8, 115.1, 68.7, 48.7, 45.3, 31.9, 30.9, 28.2, 25.9, 24.5, 22.0; HRMS (ESI-TOF) calculated for C<sub>19</sub>H<sub>21</sub>N<sub>2</sub>O<sub>5</sub>Cl<sup>+</sup> [M+H]<sup>+</sup>: 393.1212, observed 393.1222.

**4-(2-(2-(2-chloroethoxy)ethoxy)ethoxy)-2-(2,6-dioxopiperidin-3-yl)isoindoline-1,3-dione (**24**)**. Following general procedure D, tosylation was performed with 2-(2-(2-chloroethoxy)ethoxy)ethan-1-ol (1.00 g, 5.95 mmol, 1.0 eq), TsCl (1.36 g, 7.14 mmol, 1.2 eq), DMAP (219 mg, 1.79 mmol, 0.3 eq) in Pyridine (10 mL). Product was obtained as a colorless oil and was taken on crude to the next step. Continuing with general procedure D, crude Tosylate (assumed 1.61 mmol, 1.1 eq), 2-(2,6-dioxopiperidin-3-yl)-4-hydroxyisoindoline-1,3-dione (**22**) (400 mg, 1.46 mmol, 1.0 eq), KHCO<sub>3</sub> (240 mg, 2.40 mmol, 1.6 eq), KI (24.2 mg, 0.146 mmol, 0.1 eq) in DMF (10 mL). Product (**24**) was obtained as a white solid (399 mg, 58% yield). Spectral data matched the reported literature.<sup>42</sup>

**General Procedure D for the synthesis of intermediates 25 and 26.** To a solution of chloro-linker (**25** or **26**) (1.0 eq) was added DMF (0.05 M) was added NaI (10 eq) and the resulting mixture was heated to 60 °C for 20 h. Upon completion, ethyl acetate and water were added, and the layers were separated. The organic layer was washed sequentially with 10% aq LiCl, water, and brine, then dried over MgSO<sub>4</sub>. Volatiles were removed via rotary evaporation and the resulting residue was used crude in the next step of the synthesis.

**2-(2,6-dioxopiperidin-3-yl)-4-((6-iodohexyl)oxy)isoindoline-1,3-dione (**25**)** Following general procedure D, halogen exchange was performed with **23** (123 mg, 0.313 mmol, 1.0 eq), NaI (470 mg, 3.13 mmol, 10 eq) in acetone (7.5 mL). Product was obtained as a white solid (crude yield 140 mg, 92 % yield). The crude product was used in the next step of the synthesis.

**2-(2,6-dioxopiperidin-3-yl)-4-(2-(2-(2-iodoethoxy)ethoxy)ethoxy)isoindoline-1,3-dione (**26**)**. Following general procedure D, halogen exchange was performed with **24** (348 mg, 0.744 mmol, 1.0 eq), NaI (1.11 mg, 7.44 mmol, 10 equiv) in Acetone (15 mL). Product was obtained as a white solid (crude yield 331 mg, 86 % yield). The crude product was used in the next step of the synthesis. Spectral data matched the reported literature.<sup>42</sup>



**Scheme 5. Synthesis of Compound 8 and 9.**

#### General Procedure E for the synthesis of compound 8 and 9.

**Step 1:** Sulfone **20** (1.0 eq) was dissolved in a 1:1 mixture of TFA/DCM (0.08 M) and the resulting mixture was stirred at 23 °C for 2 h. Upon completion, volatiles were removed via rotary evaporation.

**Step 2:** The resulting residue was taken up in DMF (0.05M). DIEA (5 eq) and linkers **24** or **25** were added and the mixture was stirred at 80 °C for 18 hr. The reaction was allowed to cool to 23 °C, then ethyl acetate and water were added, and the layers were separated. The organic layer was washed sequentially with 10% aq LiCl, water, and brine, then dried over MgSO<sub>4</sub>. Volatiles were removed via rotary evaporation and the resulting residues were purified either purified via column chromatography (CombiFlash Rf system: 24 g silica, hexanes/ethyl acetate, 0–

100% ethyl acetate, 16 mins) or a portion of the crude material was then purified by reverse-phase HPLC.

**4-((6-(4-(3-(4-(6-((3-(1H-pyrazol-1-yl)propyl)amino)-2-(methylsulfonyl)pyrimidin-4-yl)phenoxy)propyl)piperazin-1-yl)hexyloxy)-2-(2,6-dioxopiperidin-3-yl)isoindoline-1,3-dione (8).** Following general procedure E, Sulfone **20** (49.1 mg, 0.0820 mmol, 1.0 eq) in TFA (0.50 mL) and DCM (0.50 mL) was added DIEA (71.0  $\mu$ L, 0.409 mmol, 5 eq) and **24** (51.2 mg, 0.106 mmol, 1.3 eq). Product (**8**) was purified via column chromatography (CombiFlash Rf system: 24 g silica, DCM/Methanol, 0-20% ethyl acetate, 16 mins) followed by reverse phase HPLC 0-60% ACN in 0.1% TFA H<sub>2</sub>O over 60 min affording a yellow solid (18 mg, 25 % yield). Note that HPLC purification was performed for characterization purposes of purity, the compound **8** used in the western blot studies and other binding studies were only purified by column chromatography. <sup>1</sup>H NMR (500 MHz, DMSO-*d*<sub>6</sub>)  $\delta$  11.12 (br. s, 1H), 8.16 (s, 1H), 7.99 (d, *J* = 8.3 Hz, 1H), 7.83 (dd, *J* = 8.3, 7.2 Hz, 1H), 7.76 (s, 1H), 7.52 (d, *J* = 8.5 Hz, 1H), 7.46 (d, *J* = 8.5 Hz, 2H), 7.09 (d, *J* = 8.5 Hz, 2H), 7.01 (s, 1H), 6.24 (s, 1H), 5.08 (dd, *J* = 12.9, 5.5 Hz, 1H), 4.26-4.18 (m, 2H), 4.15-4.08 (m, 2H), 3.32 (s, 3H), 2.94-2.83 (m, 2H), 2.66-2.56 (m, 2H), 2.36 (br. s, 1H), 2.12-1.95 (m, 6H), 1.79 (quintet, *J* = 5.6 Hz, 2H), 1.64 (br. m, 2H), 1.50 (quintet, *J* = 5.6 Hz, 2H), 1.39 (quintet, *J* = 5.6 Hz, 2H), 1.24 (br. m, 2H); <sup>13</sup>C NMR (100 MHz, DMSO-*d*<sub>6</sub>)  $\delta$  172.8, 170.0, 166.9, 165.4, 165.1, 138.7, 137.1, 133.3, 128.2, 119.8, 116.2, 115.3, 115.2, 114.8, 105.0, 68.8, 60.7, 59.8, 53.6, 48.8, 41.8, 32.5, 31.0, 28.5, 28.1, 25.2, 24.9, 22.0, 20.8, 18.1, 16.7, 14.1, 12.5. HRMS (ESI-TOF) calculated for C<sub>43</sub>H<sub>53</sub>N<sub>9</sub>O<sub>8</sub>S<sup>+</sup> [M+H]<sup>+</sup>: 856.3811, observed 856.3801.

**4-(2-(2-(2-(4-(3-(4-(6-((3-(1H-pyrazol-1-yl)propyl)amino)-2-(methylsulfonyl)pyrimidin-4-yl)phenoxy)propyl)piperazin-1-yl)ethoxy)ethoxy)ethoxy)-2-(2,6-dioxopiperidin-3-yl)isoindoline-1,3-dione (9).** Following general procedure E, Sulfone **20** (36.8 mg, 0.0601 mmol, 1.0 eq) in TFA (0.30 mL) and DCM (0.30 mL). Resulting residue (assumed 0.0601 mmol) in DMF (1.5 mL) was added DIEA (53.0  $\mu$ L, 0.301 mmol, 5 eq) and **24** (34.0 mg, 0.0661 mmol, 1.1 eq). Product (**9**) was purified via column chromatography (CombiFlash Rf system: 24 g silica, DCM/Methanol, 0-20% ethyl acetate, 16 mins). <sup>1</sup>H NMR (400 MHz, DMSO-*d*<sub>6</sub>)  $\delta$  11.11 (s, 1H), 7.96 (d, *J* = 7.3 Hz, 1H), 7.81 (dd, *J* = 8.4, 7.3 Hz, 1H), 7.77 (s, 1H), 7.53 (d, *J* = 8.4 Hz, 1H), 7.46 (d, *J* = 8.5 Hz, 2H), 7.07 (d, *J* = 8.5 Hz, 2H), 6.23 (s, 1H), 5.08 (dd, *J* = 12.8, 5.5 Hz, 1H), 4.34 (t, *J* = 5.2 Hz, 2H), 4.21 (t, *J* = 6.8 Hz, 1H), 4.08 (t, *J* = 5.2 Hz, 2H), 3.80 (t, *J* = 5.6 Hz, 2H), 3.66 (t, *J* = 6.0 Hz, 2H), 3.54 (t, *J* = 5.8 Hz, 2H), 3.31 (s, 3H), 3.04 (q, *J* = 7.3 Hz, 10H), 2.95-2.81 (m, 2H), 2.63-2.51 (m, 2H), 1.19 (t, *J* = 7.3 Hz, 14H); <sup>13</sup>C NMR (100 MHz, DMSO-*d*<sub>6</sub>)  $\delta$  172.8, 169.9, 166.8, 165.3, 138.6, 137.0, 133.2, 130.0, 128.2, 120.0, 116.3, 115.4, 114.8, 104.9, 70.1, 69.7, 68.9, 68.7, 48.8, 45.4, 31.0, 29.6, 22.0, 8.5; HRMS (ESI-TOF) calculated for C<sub>43</sub>H<sub>53</sub>N<sub>9</sub>O<sub>10</sub>S<sup>+</sup> [M+H]<sup>+</sup>: 888.3709, observed 888.3724.

**General procedure for AlphaScreen assay.**<sup>28</sup> His<sub>9</sub>-tagged BPTF bromodomain was expressed and purified as described previously.<sup>28</sup> His-tagged BRD9 and CECR2 were purchased from Reaction Biology (Cat. #s RD-11-214 and RD-11-210 for BRD9 and CECR2 respectively). The AlphaScreen assay

procedures were adapted from the manufacturers protocol (PerkinElmer, USA). Nickel chelate (Ni-NTA) acceptor beads and streptavidin donor beads were purchased from PerkinElmer (Cat. #: 6760619M). The biotinylated Histone H4 KAc5,8,12,16 peptide was purchased from EpiCypher (Cat. # 12-0034), with the sequence: Ac-SGRGK(Ac)GGK(Ac)GLGK(Ac)GGAK(Ac)RHRKVLR-Peg(Biot).

All reagents were diluted in the assay buffer (50 mM HEPES-Na<sup>+</sup> (ChemImpex), 100 mM NaCl (SigmaAldrich), 0.05% CHAPS (RPI), 0.1% BSA (SigmaAldrich), pH 7.4). The final assay concentrations of protein and biotinylated peptide used are shown in **Table 2**.

**Table 2: Concentrations of protein and peptide used in AlphaScreen assays**

Protein	[Protein] nM	[Peptide] nM
BPTF	30	100
BRD9	60	100
CECR2	60	100

3-fold serial dilutions were prepared with varying concentrations of the compounds and a fixed protein concentration, keeping the final DMSO concentration at 0.25%. 5  $\mu$ L of these solutions were added to a 384-well plate (ProxiPlate-384, PerkinElmer). 5  $\mu$ L of the biotinylated peptide solution was then added to the wells. 10  $\mu$ L of pre-mixed nickel chelate acceptor beads and streptavidin donor beads were added to each well under low light conditions (<100 lux), to a final concentration of 20  $\mu$ g/mL. For each test compound, BZ1 was also run as a positive control on the same plate to ensure the accuracy of the assay. The plate was sealed and incubated for 30 minutes in the dark. It was then read in AlphaScreen mode (excitation time = 100 ms, integration time = 300 ms, output: counts/s) using a Tecan Spark plate reader. Each compound was run in two technical replicates and the data was normalized against 0  $\mu$ M inhibitor signal to obtain the % normalized AlphaScreen signal. IC<sub>50</sub> values were calculated in GraphPad Prism 9 using a sigmoidal 4-parameter logistic (4PL) curve fit.

#### General procedure for in vitro ternary complex assay.

His-tagged CRBN-DDB1 protein was prepared following the procedure reported by Matyskiela et al.<sup>43</sup> GST-BPTF was purchased from BPS Biosciences (cat# 31134), while GST-BRD9, GST-CECR2, and GST-PCAF were purchased from Reactive Biology Corp (cat# RD-11-187, cat# RD-11-194, and cat# RD-11-259 respectively). All reagents were diluted in assay buffer comprising 25 mM HEPES, pH 7.4, 100 mM NaCl, 0.1% BSA, and 0.05% tween20. An ECHO 650 (Labcyte Inc.) acoustic dispenser was used to generate a 10-point dilution curve from DMSO stocks of the degraders directly into a 384-well OptiPlate (PerkinElmer, Cat. # 6007290) giving a final DMSO concentration of 0.3%. Final concentrations of His-tagged CRBN-DDB1 and GST-tagged bromodomains used in the assay are shown in **Table 3**. AlphaScreen glutathione coated donor and nickel chelate acceptor beads were purchased from PerkinElmer (Cat. # 6765300 and 6760141 respectively).

**Table 3: Concentration of proteins used in AlphaScreen ternary complex assays**

Protein	[GST-tagged]	[His-CRBN-DDB1] nM
---------	--------------	--------------------

	<b>bromodomains]</b> <b>nM</b>	
BPTF	60	120
BRD9	240	80
CECR2	240	80
PCAF	240	80

Briefly, to a 384-well OptiPlate containing 5X degrader in triplicate was added 5  $\mu$ L of a 5X solution of His-CRBN-DDB1 and GST-tagged bromodomain and then incubated at rt for 1 h. After incubation, 10  $\mu$ L nickel chelate acceptor (20  $\mu$ L/mL final concentration) and 10  $\mu$ L glutathione donor beads (20  $\mu$ L/mL final concentration) were added. The plate was sealed and mixed on a MixMate (eppendorf) for 1 h at rt and then luminescence detection was collected on an Envision plate reader (PerkinElmer).

**In-cell NanoBRET assay.** NanoBRET experiments were carried out using the NanoBRET CRBN Ternary Complex Starter Kit (Cat # ND2720) according to the manufacturer's protocol (Promega NanoBRET™ CRBN Ternary Complex Assay TM615).<sup>44</sup> All assays were run in 384-well format. HEK293T cells were transfected to a 1:100 donor:acceptor (Nluc:Halotag vectors) ratio for both BPTF-BD and BRD9-FL vectors (see supporting information for the design of plasmids). Cells were re-plated, treated with the HaloTag 618 Ligand and treated with compounds as described in the manufacturer's procedure. Data was collected on a Tecan Spark plate reader using the settings in **Table 4**.

**Table 4: Tecan Spark settings for NanoBRET experiments**

1) Shaking (Linear)	Duration [s] 30 Amplitude [mm] 1 Frequency [rpm] 1440
2) Mode: Luminescence Multi Color	
Donor Emission	Wavelength start = 445 nm Wavelength end = 470 nm Integration time = 300 ms
Acceptor Emission	Wavelength start = 610 nm Wavelength end = 700 nm Integration time = 300 ms

**Competition with monovalent inhibitor for ternary complex formation:** For competition experiments (**Figure S4**), 10X solutions of compound **19** and MG-132 were prepared in OptiMEM® I Reduced Serum Medium and pre-mixed in tubes. 10  $\mu$ L of this solution was then added to each well. The plates were incubated for 30 minutes, followed by the addition of degrader compounds. The rest of the assay was carried out according to the technical manual referenced above.

**Cell culture.** HEK293T cells were grown in a humidified 5% CO<sub>2</sub> environment at 37 °C. Cells were cultured in DMEM media (high-glucose, Gibco Cat.# 11965-092) supplemented with 10% fetal-bovine serum (Cellgro Cat.# QB-110-001-101), Penicillin-Streptomycin (50 U/mL penicillin, 50  $\mu$ g/mL streptomycin, Cellgro Cat.# 15140-122). The cells were passaged to a 1:20 dilution by decanting suspended cells and dissociating

adherent cells from cell culture flasks in 0.25% trypsin/ EDTA (Gibco, Cat.# 25200056) after 1 min incubation.

**Western blotting.** HEK293T cells were seeded at a density of  $5 \times 10^5$  cells per well in 6-well plates in 2.5 mL of medium. At 80-90% confluency, 250  $\mu$ L of the medium was removed from each well and the cells were treated with compounds at the desired concentrations for indicated times, to a final DMSO concentration of 0.1% v/v. For collecting lysates, the medium was removed and the wells were rinsed with 1 mL of ice-cold PBS, followed by the addition of 100  $\mu$ L cold RIPA buffer (ThermoFisher Cat.# 89900) supplemented with cComplete Mini Protease Inhibitor cocktail (Roche Cat.# 11836153001). The plates were incubated on ice for 15 min. After high-speed centrifugation (15,000g for 15 minutes), the supernatant was collected and protein concentrations were determined by the BCA assay (ThermoFisher Cat.# 23227). The samples were normalized by total protein content, mixed with 4 $\times$  NuPAGE LDS loading buffer (Invitrogen) and heated at 100 °C for 10 minutes.

Proteins were resolved by SDS-PAGE on NuPage 4–12% Bis-Tris (for CECR2, BRD9 and PCAF) or 3–8% Tris-acetate gels (for BPTF) (Invitrogen Cat.# NP0323BOX, EA03785BOX) and transferred to PVDF membrane (Bio-rad Cat.# 1620174) using wet transfer for 60 minutes. Membranes were dried, blocked in TBS-T (Tris-buffered saline-T) containing 5% w/v nonfat dry milk for 1 h at room temperature. They were subsequently incubated with primary antibodies at dilutions and times in **Table S1**. After the membranes were washed five times with TBS-T, they were incubated with secondary antibodies at dilutions and times listed below. Finally, the membranes were washed five times in TBS-T and treated with SuperSignal West Dura substrates (ThermoFisher Cat.# 34095) and imaged using a Bio-rad Chemi-Doc imaging system.

## ASSOCIATED CONTENT

**Supporting Information.** Characterization data of small molecules, biophysical and cellular assays data. The Supporting Information is available free of charge at <http://pubs.acs.org>.

## AUTHOR INFORMATION

### Corresponding Author

\*William C.K. Pomerantz  
Department of Chemistry, University of Minnesota, Minneapolis, Minnesota 55455, United States; Department of Medicinal Chemistry, University of Minnesota, Minneapolis, Minnesota 55455, United States; orcid.org/0000-0002-0163-4078;  
Email: wcp@umn.edu

### Author Contributions

H.Z., J.P.C. and J.R.K. designed and synthesized the compounds; H.Z. and J.P.C. performed AlphaScreen assays; M.A. performed the in vitro ternary complex assay; H.Z. and J.P.C. performed cellular experiments; Z.R. and W.C.K.P. oversaw the experiments and interpretation of data; H.Z., J.P.C. and W.C.K.P. wrote the manuscript. <sup>‡</sup>These authors contributed equally to the manuscript.

### Funding Sources

This work was supported by the NIH MIRA award R35 GM140837-01 (W.C.K.P.), St. Jude Children's Research Hospital (M.A. and Z.R.) and the National Institutes of Health's National Center for Advancing Translational Sciences, grant UL1TR002494. The content is solely the responsibility of the

authors and does not necessarily represent the official views of the National Institutes of Health's National Center for Advancing Translational Sciences. Additional support was provided by The Pediatric Device Innovation Consortium at the University of Minnesota. H.Z. was supported by the University of Minnesota Doctoral Dissertation Fellowship 2020 and J.R.K. by the NIH NRSA 1 F32 CA261169-01

## Notes

W.C.K.P., H.Z., J.P.C. and J.R.K. at the University of Minnesota have filed a provisional patent application on the degraders disclosed in this report. Z.R. receives consulting fees from Revolution Medicines, Orum Therapeutics and Nyrada Inc.

## ACKNOWLEDGMENT

The authors would like to thank Caroline Buchholz for optimizing the AlphaScreen assays for BRD9 and CECR2 bromodomains and Prakriti Kalra for helping with the design of NanoBRET plasmid constructs.

Figures were created with BioRender and PyMOL.

Figure 1B was adapted with permission from Springer Nature, Applied Biophysics for Bromodomain Drug Discovery by William C. K. Pomerantz, Jordan A. Johnson, Peter D. Ycas Copyright 2019.

## ABBREVIATIONS

BAF, BRG1/BRM-associated factor; BD, bromodomain; BET, bromodomain and extraterminal; BPTF, bromodomain PHD-finger transcription factor; BRD9, bromodomain-containing protein 9; BRET, bioluminescence resonance energy transfer; CECR2, cat eye syndrome chromosome region candidate 2; CRBN, cereblon; FL, full-length; GCN5, general control non-depressible 5; ISWI, imitation switch; Nluc, nanoluciferase; NURF, nucleosome remodeling factor; PBAF, polybromo-associated BAF; PCAF, p300/CBP-associated factor; PEG, polyethylene glycol; SAR, structure-activity relationship.

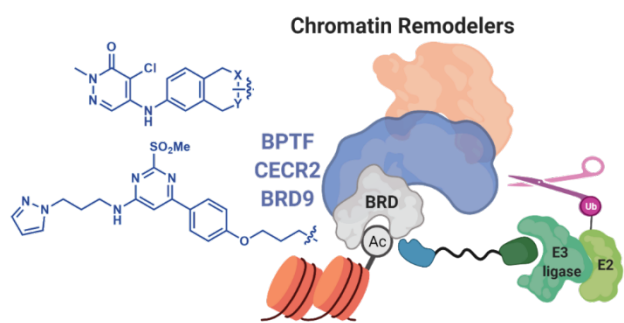
## REFERENCES

- Saha, A.; Wittmeyer, J.; Cairns, B. R. Chromatin Remodelling: The Industrial Revolution of DNA around Histones. *Nat. Rev. Mol. Cell Biol.* **2006**, *7* (6), 437–447.
- Clapier, C. R.; Iwasa, J.; Cairns, B. R.; Peterson, C. L. Mechanisms of Action and Regulation of ATP-Dependent Chromatin-Remodelling Complexes. *Nat. Rev. Mol. Cell Biol.* **2017**, *18* (7), 407–422.
- Nair, S. S.; Kumar, R. Chromatin Remodeling in Cancer: A Gateway to Regulate Gene Transcription. *Mol. Oncol.* **2012**, *6* (6), 611–619.
- Wang, X.; Wang, S.; Troisi, E. C.; Howard, T. P.; Haswell, J. R.; Wolf, B. K.; Hawk, W. H.; Ramos, P.; Oberlick, E. M.; Tzvetkov, E. P.; Vazquez, F.; Hahn, W. C.; Park, P. J.; Roberts, C. W. M. BRD9 Defines a SWI/SNF Sub-Complex and Constitutes a Specific Vulnerability in Malignant Rhabdoid Tumors. *Nat. Commun.* **2019**, *10* (1), 1–11.
- Kaaser, M. D.; Aslanian, A.; Dong, M.-Q.; Yates, J. R.; Emerson, B. M. BRD7, a Novel PBAF-Specific SWI/SNF Subunit, Is Required for Target Gene Activation and Repression in Embryonic Stem Cells. *J. Biol. Chem.* **2008**, *283* (47), 32254–32263.
- Syntichaki, P.; Topalidou, I.; Thireos, G. The Gcn5 Bromodomain Co-Ordinates Nucleosome Remodelling. *Nature* **2000**, *404* (6776), 414–417.
- Li, Y.; Gong, H.; Wang, P.; Zhu, Y.; Peng, H.; Cui, Y.; Li, H.; Liu, J.; Wang, Z. The Emerging Role of ISWI Chromatin Remodeling Complexes in Cancer. *J. Exp. Clin. Cancer Res.* **2021**, *40* (1), 346.
- Xiao, H.; Sandaltzopoulos, R.; Wang, H.-M.; Hamiche, A.; Ranallo, R.; Lee, K.-M.; Fu, D.; Wu, C. Dual Functions of Largest NURF Subunit NURF301 in Nucleosome Sliding and Transcription Factor Interactions. *Mol. Cell* **2001**, *8* (3), 531–543.
- Banting, G. S.; Barak, O.; Ames, T. M.; Burnham, A. C.; Kardel, M. D.; Cooch, N. S.; Davidson, C. E.; Godbout, R.; McDermid, H. E.; Shiekhata, R. CECR2, a Protein Involved in Neurulation, Forms a Novel Chromatin Remodeling Complex with SNF2L. *Hum. Mol. Genet.* **2005**, *14* (4), 513–524.
- Kumar, R.; Li, D.-Q.; Müller, S.; Knapp, S. Epigenomic Regulation of Oncogenesis by Chromatin Remodeling. *Oncogene* **2016**, *35* (34), 4423–4436.
- Clegg, M. A.; Tomkinson, N. C. O.; Prinjha, R. K.; Humphreys, P. G. Advancements in the Development of Non-BET Bromodomain Chemical Probes. *ChemMedChem* **2019**, *14* (4), 362–385.
- Zahid, H.; Buchholz, C. R.; Singh, M.; Ciccone, M. F.; Chan, A.; Nithianantham, S.; Shi, K.; Aihara, H.; Fischer, M.; Schönbrunn, E.; dos Santos, C. O.; Landry, J. W.; Pomerantz, W. C. K. New Design Rules for Developing Potent Cell-Active Inhibitors of the Nucleosome Remodeling Factor (NURF) via BPTF Bromodomain Inhibition. *J. Med. Chem.* **2021**, *64* (18), 13902–13917.
- Mélin, L.; Calosing, C.; Kharenko, O. A.; Hansen, H. C.; Gagnon, A. Synthesis of NVS-BPTF-1 and Evaluation of Its Biological Activity. *Bioorg. Med. Chem. Lett.* **2021**, *47* (June), 128208.
- Tyutyunyk-Massey, L.; Sun, Y.; Dao, N.; Ngo, H.; Dammalapati, M.; Vaidyanathan, A.; Singh, M.; Haqqani, S.; Haueis, J.; Finnegan, R.; Deng, X.; Kirberger, S. E.; Bos, P. D.; Bandyopadhyay, D.; Pomerantz, W. C. K.; Pommier, Y.; Gewirtz, D. A.; Landry, J. W. Autophagy-Dependent Sensitization of Triple-Negative Breast Cancer Models to Topoisomerase II Poisons by Inhibition of The Nucleosome Remodeling Factor. *Mol. Cancer Res.* **2021**.
- Vogelmann, A.; Robaa, D.; Sippl, W.; Jung, M. Proteolysis Targeting Chimeras (PROTACs) for Epigenetics Research. *Curr. Opin. Chem. Biol.* **2020**, *57*, 8–16.
- Brien, G. L.; Remillard, D.; Shi, J.; Hemming, M. L.; Chabon, J.; Wynne, K.; Dillon, E. T.; Cagney, G.; Van Mierlo, G.; Baltissen, M. P.; Vermeulen, M.; Qi, J.; Fröhling, S.; Gray, N. S.; Bradner, J. E.; Vakoc, C. R.; Armstrong, S. A. Targeted Degradation of BRD9 Reverses Oncogenic Gene Expression in Synovial Sarcoma. *Elife* **2018**, *7*, 1–26.
- Bassi, Z. I.; Fillmore, M. C.; Miah, A. H.; Chapman, T. D.; Maller, C.; Roberts, E. J.; Davis, L. C.; Lewis, D. E.; Galwey, N. W.; Waddington, K. E.; Parravicini, V.; Macmillan-Jones, A. L.; Gongora, C.; Humphreys, P. G.; Churcher, I.; Prinjha, R. K.; Tough, D. F. Modulating PCAF/GCN5 Immune Cell Function through a PROTAC Approach. *ACS Chem. Biol.* **2018**, *13* (10), 2862–2867.
- Pomerantz, W. C. K.; Johnson, J. A.; Ycas, P. D. Applied Biophysics for Bromodomain Drug Discovery; 2019; pp 287–337.
- Gadd, M. S.; Testa, A.; Lucas, X.; Chan, K.-H.; Chen, W.; Lamont, D. J.; Zengerle, M.; Ciulli, A. Structural Basis of PROTAC Cooperative Recognition for Selective Protein Degradation. *Nat Chem Biol* **2017**, *13* (5), 514–521.
- Divakaran, A.; Zahid, H.; Lin, W.; Chen, T.; Harki, D. A.; Pomerantz, W. C. K. Development of an N-Terminal BRD4 Bromodomain-Targeted Degradator. *ChemRxiv* **2021**, Preprint-not peer reviewed.
- Richart, L.; Carrillo-de Santa Pau, E.; Río-Machín, A.; de Andrés, M. P.; Cigudosa, J. C.; Lobo, V. J. S.-A.; Real, F. X. BPTF Is Required for C-MYC Transcriptional Activity and in Vivo Tumorigenesis. *Nat. Commun.* **2016**, *7* (1), 10153.
- Green, A. L.; DeSisto, J.; Flannery, P.; Lemma, R.; Knox, A.; Lemieux, M.; Sanford, B.; O'Rourke, R.; Ramkissoon, S.; Jones, K.; Perry, J.; Hui, X.; Moroze, E.; Balakrishnan, I.; O'Neill, A. F.; Dunn, K.; DeRyckere, D.; Danis, E.; Safadi, A.; Gilani, A.; Hubbell-Engler, B.; Nuss, Z.; Levy, J. M. M.; Serkova, N.; Venkataraman, S.; Graham, D. K.; Foreman, N.; Ligon, K.; Jones, K.; Kung, A. L.; Vibhakar, R. BPTF Regulates Growth of Adult and Pediatric High-Grade Glioma through the MYC Pathway. *Oncogene* **2020**, *39* (11), 2305–2327.
- Zhang, M.; Liu, Z. Z.; Aoshima, K.; Cai, W. L.; Sun, H.; Xu, T.; Zhang, Y.; An, Y.; Chen, J. F.; Chan, L. H.; Aoshima, A.; Lang,

- S. M.; Tang, Z.; Che, X.; Li, Y.; Rutter, S. J.; Bossuyt, V.; Chen, X.; Morrow, J. S.; Pusztai, L.; Rimm, D. L.; Yin, M.; Yan, Q. CECR2 Drives Breast Cancer Metastasis by Promoting NF-KB Signaling and Macrophage-Mediated Immune Suppression. *Sci. Transl. Med.* **2022**, *14* (630), eabf5473.
- (24) Humphreys, P. G.; Bamborough, P.; Chung, C. W.; Craggs, P. D.; Gordon, L.; Grandi, P.; Hayhow, T. G.; Hussain, J.; Jones, K. L.; Lindon, M.; Michon, A. M.; Renaux, J. F.; Suckling, C. J.; Tough, D. F.; Prinjha, R. K. Discovery of a Potent, Cell Penetrant, and Selective P300/CBP-Associated Factor (PCAF)/General Control Nonderepressible 5 (GCN5) Bromodomain Chemical Probe. *J. Med. Chem.* **2017**, *60* (2), 695–709.
- (25) Structural Genomics Consortium. TP-238 A chemical probe for CECR2/BPTF bromodomains <https://www.thesgc.org/chemical-probes/TP-238>.
- (26) Lu, H.; Lu, T.; Zu, S.; Duan, Z.; Guang, Y.; Li, Q.; Ma, J.; Chen, D.; Li, B.; Lu, W.; Jiang, H.; Luo, C.; Ye, D.; Chen, K.; Lin, H. Discovery of a Highly Potent CECR2 Bromodomain Inhibitor with 7H-Pyrrolo[2,3-d] Pyrimidine Scaffold. *Bioorg. Chem.* **2022**, *123*, 105768.
- (27) Troup, R. I.; Fallan, C.; Baud, M. G. J. Current Strategies for the Design of PROTAC Linkers: A Critical Review. *Explor. Target. Anti-tumor Ther.* **2020**, *1* (5), 273–312.
- (28) Ycas, P. D.; Zahid, H.; Chan, A.; Olson, N. M.; Johnson, J. A.; Talluri, S. K.; Schonbrunn, E.; Pomerantz, W. C. K. New Inhibitors for the BPTF Bromodomain Enabled by Structural Biology and Biophysical Assay Development. *Org. Biomol. Chem.* **2020**, *18* (27), 5174–5182.
- (29) Casement, R.; Bond, A.; Craigon, C.; Ciulli, A. Mechanistic and Structural Features of PROTAC Ternary Complexes; 2021; pp 79–113.
- (30) Hu, Z.; Crews, C. M. Recent Developments in PROTAC-Mediated Protein Degradation: From Bench to Clinic. *ChemBioChem* **2022**, *23* (2).
- (31) Machleidt, T.; Woodroffe, C. C.; Schwinn, M. K.; Méndez, J.; Robers, M. B.; Zimmerman, K.; Otto, P.; Daniels, D. L.; Kirkland, T. A.; Wood, K. V. NanoBRET—A Novel BRET Platform for the Analysis of Protein–Protein Interactions. *ACS Chem. Biol.* **2015**, *10* (8), 1797–1804.
- (32) Cecchini, C.; Pannilunghi, S.; Tardy, S.; Scapozza, L. From Conception to Development: Investigating PROTACs Features for Improved Cell Permeability and Successful Protein Degradation. *Front. Chem.* **2021**, *9* (April), 1–23.
- (33) Auld, D. S.; Inglese, J. *Interferences with Luciferase Reporter Enzymes*; 2004.
- (34) Clegg, M. A.; Bamborough, P.; Chung, C.; Craggs, P. D.; Gordon, L.; Grandi, P.; Leveridge, M.; Lindon, M.; Liwicki, G. M.; Michon, A.-M.; Molnar, J.; Rioja, I.; Soden, P. E.; Theodoulou, N. H.; Werner, T.; Tomkinson, N. C. O.; Prinjha, R. K.; Humphreys, P. G. Application of Atypical Acetyl-Lysine Methyl Mimetics in the Development of Selective Inhibitors of the Bromodomain-Containing Protein 7 (BRD7)/Bromodomain-Containing Protein 9 (BRD9) Bromodomains. *J. Med. Chem.* **2020**, *63* (11), 5816–5840.
- (35) Remillard, D.; Buckley, D. L.; Paulk, J.; Brien, G. L.; Sonnett, M.; Seo, H.-S.; Dastjerdi, S.; Wühr, M.; Dhe-Paganon, S.; Armstrong, S. A.; Bradner, J. E. Degradation of the BAF Complex Factor BRD9 by Heterobifunctional Ligands. *Angew. Chemie Int. Ed.* **2017**, *56* (21), 5738–5743.
- (36) Muñoz Velasco, R.; Jiménez Sánchez, P.; García García, A.; Blanco Martínez-Illescas, R.; Pastor Senovilla, Á.; Lozano Yagüe, M.; Trento, A.; García-Martin, R. M.; Navarro, D.; Sainz, B.; Rodríguez Peralto, J. L.; Sánchez-Arévalo Lobo, V. J. Targeting BPTF Sensitizes Pancreatic Ductal Adenocarcinoma to Chemotherapy by Repressing ABC-Transporters and Impairing Multidrug Resistance (MDR). *Cancers (Basel)*. **2022**, *14* (6), 1518.
- (37) Carlson, A. S.; Cui, H.; Divakaran, A.; Johnson, J. A.; Brunner, R. M.; Pomerantz, W. C. K.; Topczewski, J. J. Systematically Mitigating the P38 $\alpha$  Activity of Triazole-Based BET Inhibitors. *ACS Med. Chem. Lett.* **2019**, *10* (9), 1296–1301.
- (38) Remillard, D.; Buckley, D. L.; Paulk, J.; Brien, G. L.; Sonnett, M.; Seo, H.-S.; Dastjerdi, S.; Wühr, M.; Dhe-Paganon, S.; Armstrong, S. A.; Bradner, J. E. Degradation of the BAF Complex Factor BRD9 by Heterobifunctional Ligands. *Angew. Chemie Int. Ed.* **2017**, *56* (21), 5738–5743.
- (39) Olson, N. M.; Kroc, S.; Johnson, J. A.; Zahid, H.; Ycas, P. D.; Chan, A.; Kimbrough, J. R.; Kalra, P.; Schönbrunn, E.; Pomerantz, W. C. K. NMR Analyses of Acetylated H2A.Z Isoforms Identify Differential Binding Interactions with the Bromodomain of the NURF Nucleosome Remodeling Complex. *Biochemistry* **2020**, *59* (20), 1871–1880.
- (40) Tahirovic, Y. A.; Truax, V. M.; Wilson, R. J.; Jecs, E.; Nguyen, H. H.; Miller, E. J.; Kim, M. B.; Kuo, K. M.; Wang, T.; Sum, C. S.; Cvijic, M. E.; Schroeder, G. M.; Wilson, L. J.; Liotta, D. C. Discovery of N -Alkyl Piperazine Side Chain Based CXCR4 Antagonists with Improved Drug-like Properties. *ACS Med. Chem. Lett.* **2018**, *9* (5), 446–451.
- (41) Devender, M.; Sravanthi, Chada Umapathi, N.; Jalapathi, P. A Facile Synthesis, Characterization of N-Substituted 7-Methoxy-3-Phenyl-4-(3-Piperizin-1-Yl-Propoxy) Chromen-2-One. *Der Pharma Chem.* **2012**, *4* (5), 2029–2035.
- (42) Rana, S.; Bendjennat, M.; Kour, S.; King, H. M.; Kizhake, S.; Zahid, M.; Natarajan, A. Selective Degradation of CDK6 by a Palbociclib Based PROTAC. *Bioorg. Med. Chem. Lett.* **2019**, *29* (11), 1375–1379.
- (43) Matyskiela, M. E.; Lu, G.; Ito, T.; Pagarigan, B.; Lu, C.-C.; Miller, K.; Fang, W.; Wang, N.-Y.; Nguyen, D.; Houston, J.; Carmel, G.; Tran, T.; Riley, M.; Nosaka, L.; Lander, G. C.; Gaidarova, S.; Xu, S.; Ruchelman, A. L.; Handa, H.; Carmichael, J.; Daniel, T. O.; Cathers, B. E.; Lopez-Girona, A.; Chamberlain, P. P. A Novel Cereblon Modulator Recruits GSPT1 to the CRL4CRBN Ubiquitin Ligase. *Nature* **2016**, *535* (7611), 252–257.
- (44) Mahan, S. D.; Riching, K. M.; Urh, M.; Daniels, D. L. Kinetic Detection of E3:PROTAC:Target Ternary Complexes Using Technology in Live Cells; 2021; pp 151–171.

---

Table of Contents graphic:





## Supporting Information

### Design of Class I/IV non-BET Bromodomain-Targeting Degraders

Huda Zahid,<sup>‡,a</sup> Jeff P. Costello,<sup>‡,a</sup> Jennifer R. Kimbrough,<sup>a</sup> Marisa Actis,<sup>c</sup> Zoran Rankovic,<sup>c</sup>  
William C. K. Pomerantz<sup>\*,a,b</sup>

<sup>a</sup>Department of Chemistry, University of Minnesota, 207 Pleasant St. SE, Minneapolis, Minnesota 55455, United States

<sup>b</sup>Department of Medicinal Chemistry, University of Minnesota, 308 Harvard Street SE, Minneapolis, Minnesota 55455, United States

<sup>c</sup>Department of Chemical Biology & Therapeutics, St. Jude Children's Research Hospital, Memphis, TN 38105, United States

<sup>‡</sup>These authors contributed equally to the manuscript.

Corresponding Author: \*William C.K. Pomerantz, email: wcp@umn.edu

### Contents

<b>AlphaScreen titrations of inhibitors and degraders</b> .....	2
<b>NanoBRET data</b> .....	2
<b>Western Blotting data</b> .....	4
<b>Analytical HPLC traces of compounds 3-6 and 8-10</b> .....	6
<b><sup>1</sup>H and <sup>13</sup>C NMR spectra of small molecules</b> .....	9

### AlphaScreen titrations of inhibitors and degraders

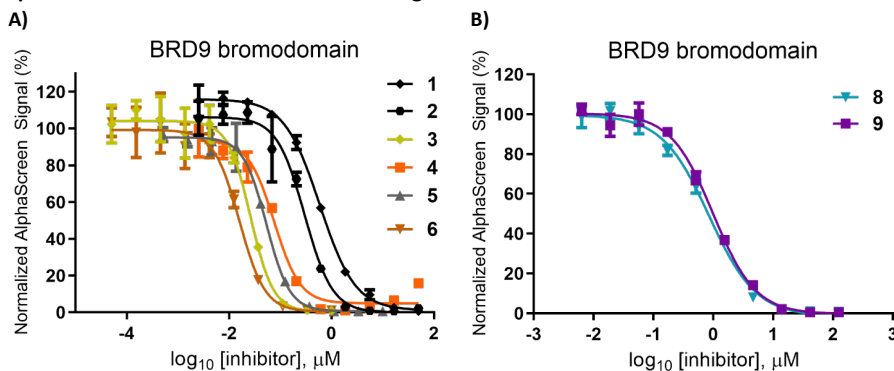


Figure S1: AlphaScreen titration of BRD9 bromodomain with **A)** Compounds 1-6 and **B)** 7-9

Commented [HZ1]: Add TP-238 data in Figure S1B when Jeff gets it

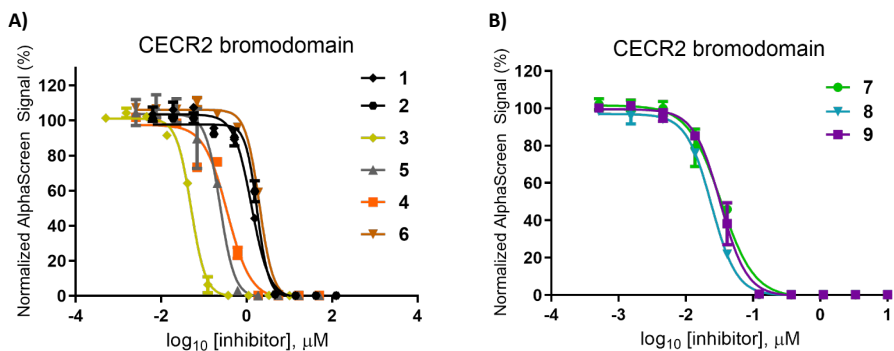


Figure S2: AlphaScreen titration of CECR2 bromodomain with **A)** Compounds 1-6 and **B)** 7-9

### NanoBRET data

**Design of BPTF-BD-Nluc plasmids:** The vector backbones pNLF1-N [CMV/Hygro] (GenBank® Accession Number KF811457) and pNLF1-C [CMV/Hygro] (GenBank® Accession Number KF811458) were obtained from Promega. The following BPTF -BD sequence was cloned into the multiple cloning region through Genscript:

SMSTEDAMTVLTPLEKDYEGLKRVLRLSLQAHKMAWPFLEPVDPNADPDYGVIKPEMDLATMEERVQRYYEKLTEF  
VADMTKIFDNCRYNPSDSPFYQCAEVLESFFVQKLKGFKASRSH

**BRD9-FL-Nluc** (CS1679C145) and **Halotag-CRBN** (N2691) fusion vectors were purchased from Promega.

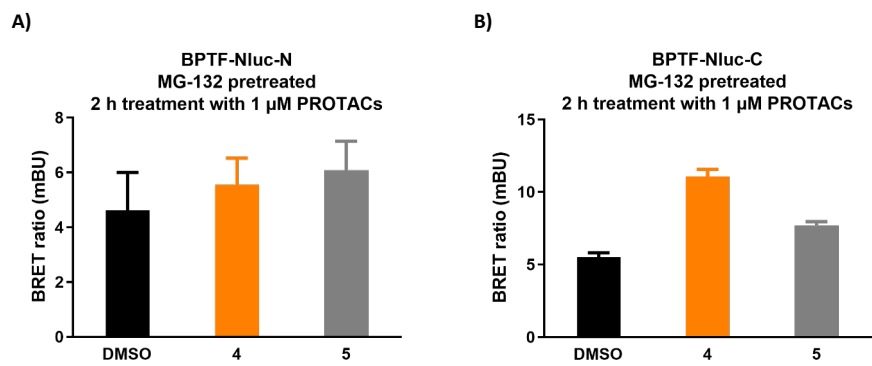


Figure S3: Ternary complex formation via NanoBRET with A) N- and B) C-terminal fusions of Nluc with BPTF bromodomain (BD). Each compound was run in three technical replicates.

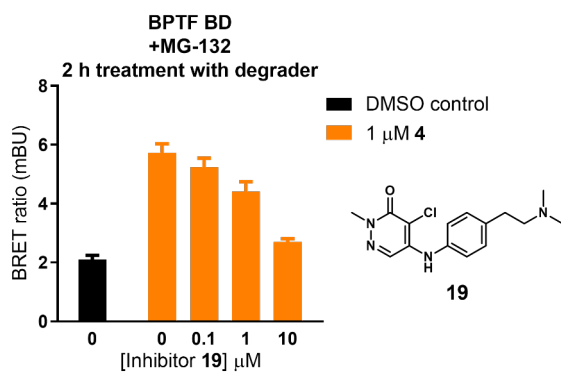


Figure S4: Competition experiments with varying concentrations of the monovalent inhibitor 19

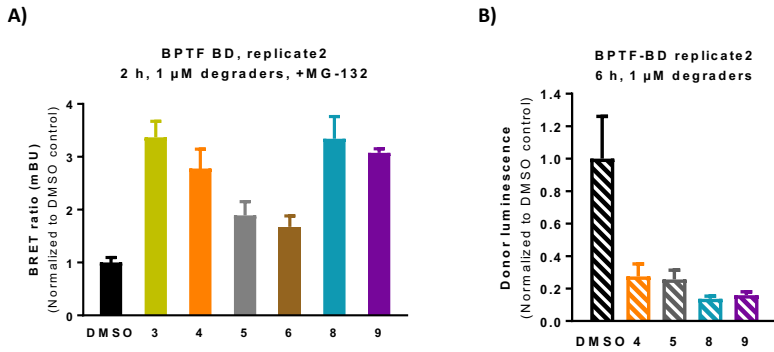


Figure S5: NanoBRET second experimental replicate for **A)** BPTF-BD ternary complex formation in Figure 4B and **B)** BPTF-BD degradation in Figure 4C. Three technical replicates.

Commented [HZ2]: Add TP-238 reps in A) and B)

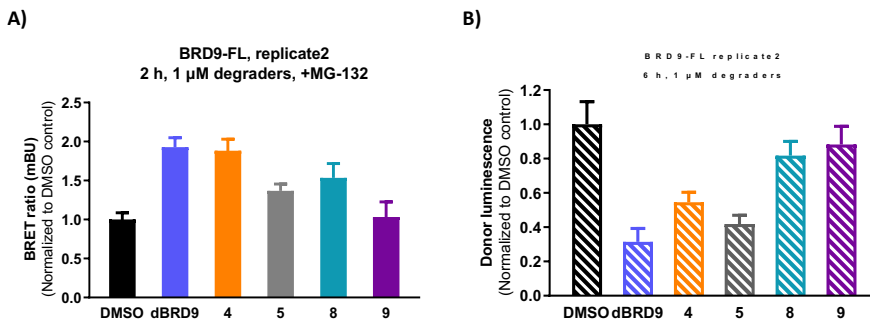


Figure S6: NanoBRET second experimental replicate for **A)** BRD9-FL ternary complex formation in Figure 5A and **B)** BRD9-FL degradation in Figure 5C. Three technical replicates.

Commented [HZ3]: Add TP reps in B

## Western Blotting data

Table S1: Antibodies used for western blotting

Target	Species	Manufacturer	Cat. #	Dilution	Incubation time	Conjugate
<b>Primary Antibodies</b>						
BPTF	Rabbit	Millipore Sigma	MLL-ABE24	1:1000	1 h RT or overnight at 4 °C	
CECR2	Rabbit	LSBio	LS-C496852	1:500	1 h RT or overnight at 4 °C	
BRD9	Rabbit	Bethyl	A303-781A	1:1000	1 h RT or overnight 4 °C	
PCAF	Rabbit	Cell Signaling	C14G9	1:1000	1 h RT or overnight 4 °C	

Vinculin	Mouse	Invitrogen	14-9777-82	1:2000	30 min RT	
$\beta$ -actin	Mouse	Invitrogen	MA5-11869	1:2000	30 min RT	
<b>Secondary Antibodies</b>						
Mouse	Goat	Invitrogen	G-21040	1:10,000	1 h RT	HRP
Rabbit	Goat	Invitrogen	G-31460	1:1000	1 h RT	HRP

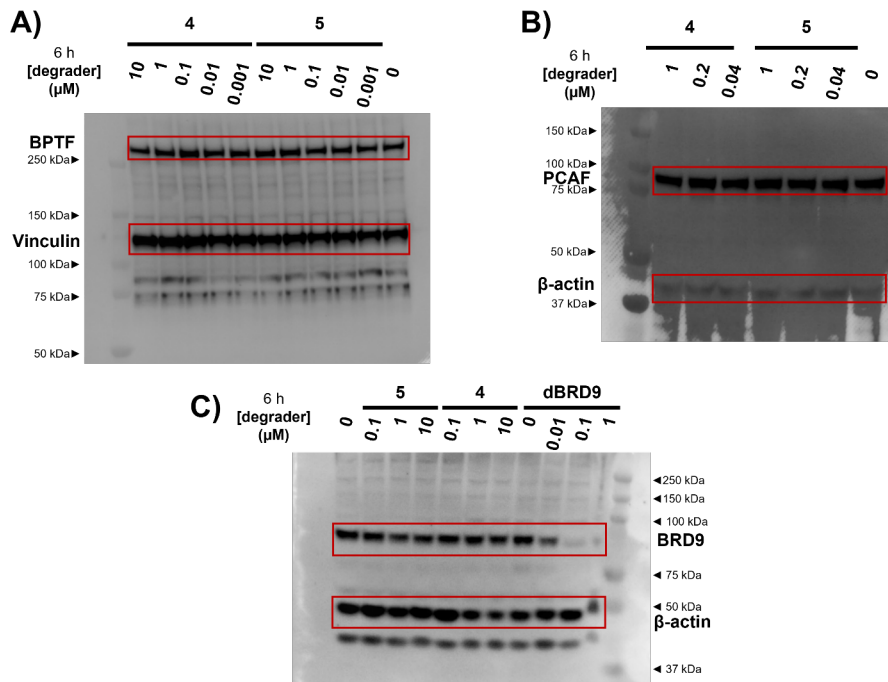


Figure S7: Western blots of compounds 4 and 5 with A) BPTF, B) PCAF and C) BRD9 (with dBRD9 as a positive control) in HEK293T cells treated for 6 h.

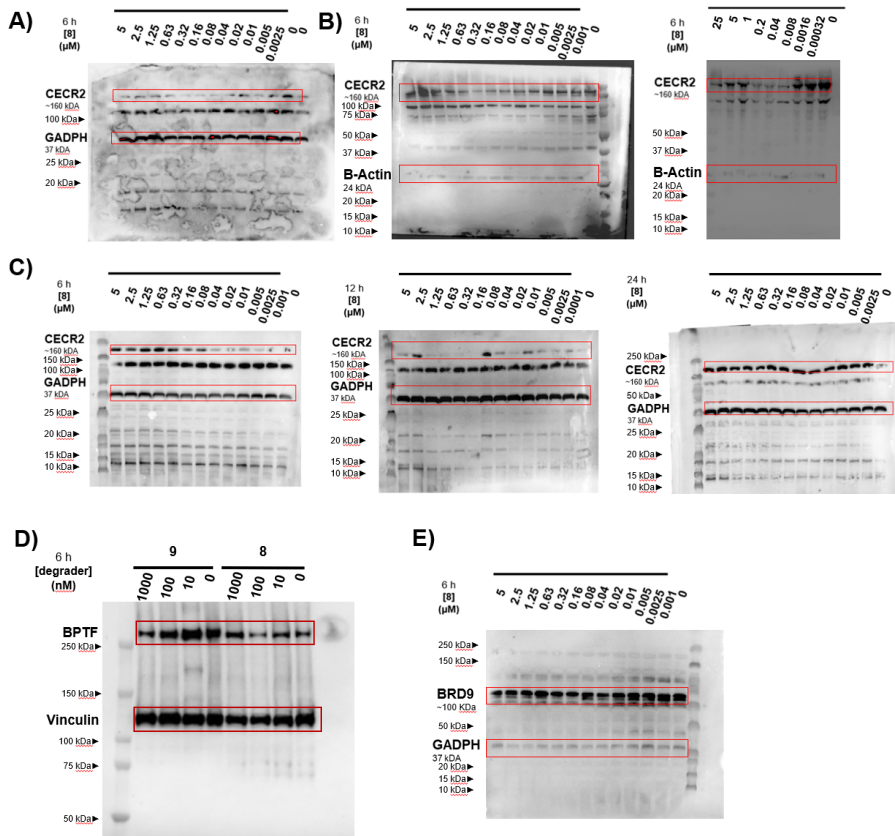
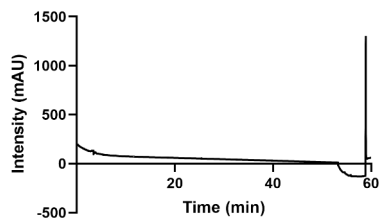


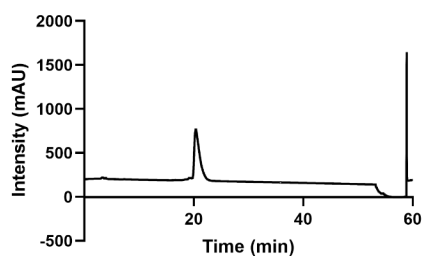
Figure S8: Western blots of compounds **8** with **A)** CECR2, GADPH loading control, 6 h treatment. **B)** CECR2,  $\beta$ -Actin loading control 6 h exposure. *Note: CECR2 antibody appeared to interfere with  $\beta$ -Actin. Blots were nonetheless included with similar degradation patterns to A) and C).* **C)** CECR2, GADPH loading control time HEK293T cells treated and analyzed at 6, 12 and, 24 h time points. Western blots of compound **8** and **9** with **D)** BPTF and **E)** BRD9.

Analytical HPLC traces of compounds 3-6 and 8-10

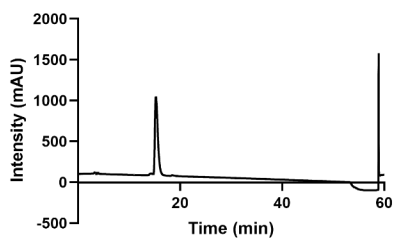
A) Blank 3-6



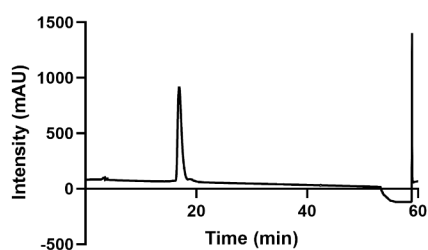
B) Compound 3



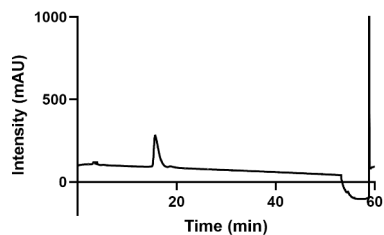
C) Compound 4



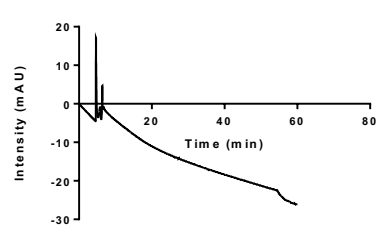
D) Compound 5



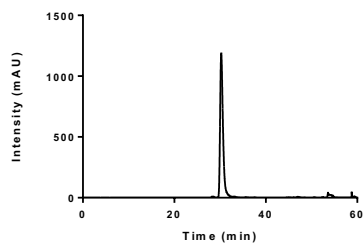
D) Compound 6



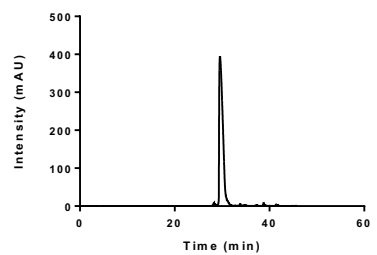
E) Blank 8, 9



**F) Compound 8**



**G) Compound 9**



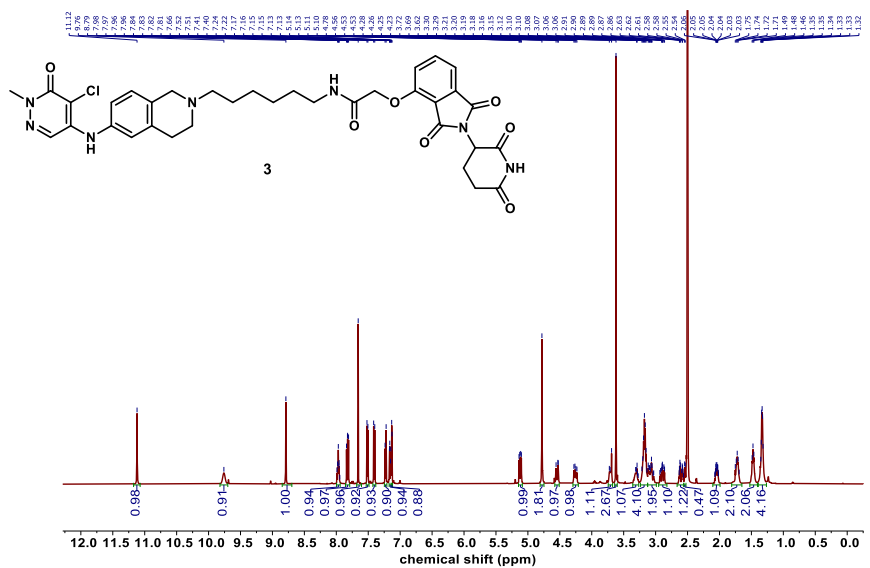
Compound	% Purity
3	96.2
4	97.0
5	96.9
6	98.3
8	96.1
9	95.6

Figure S9: HPLC spectra at 272 nm of **A)** Blank **B) 3, C) 4, D) 5, E) 6** over a gradient of 5-40% ACN in 0.1%TFA (aq) for compounds **3, 5** and **6** and 5-60% ACN in 0.1%TFA (aq) for compound **4**. % Purity calculated from 0-50 min (excluding the solvent front).

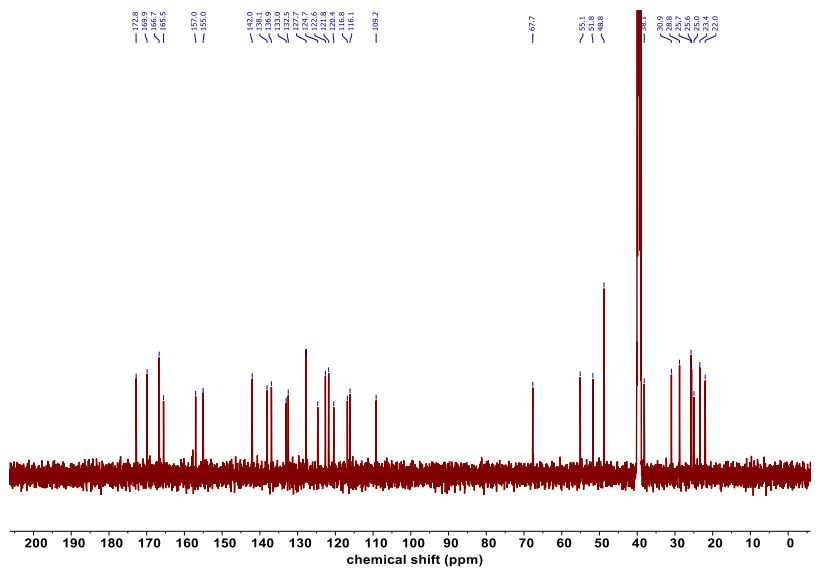


### <sup>1</sup>H and <sup>13</sup>C NMR spectra of small molecules

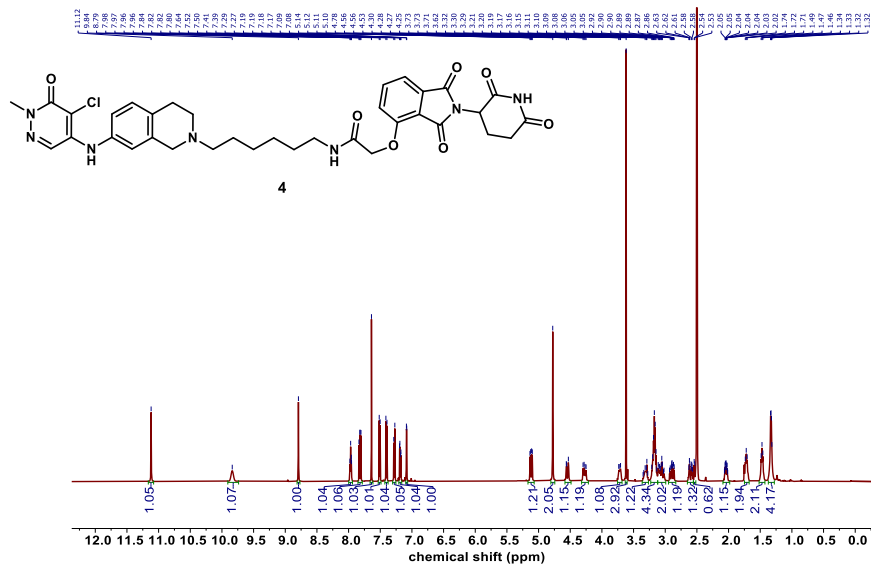
**3**, <sup>1</sup>H NMR (500 MHz, DMSO-d<sub>6</sub>)



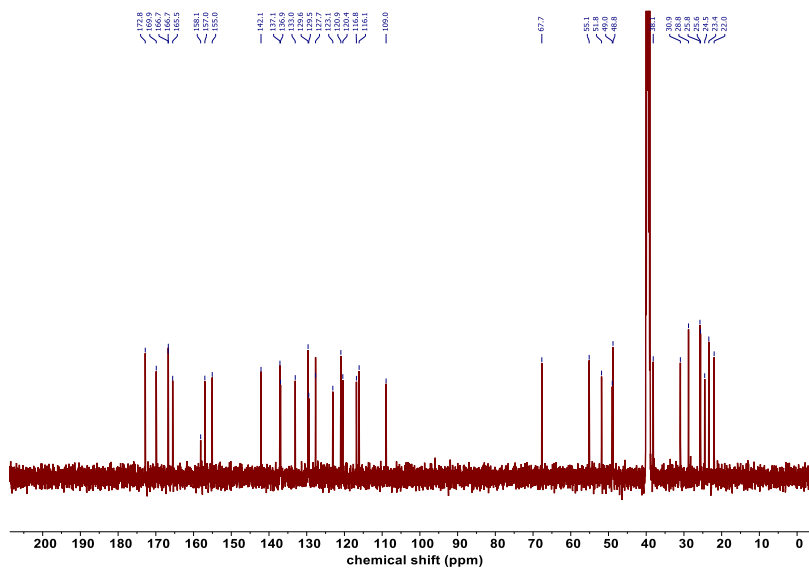
**3**, <sup>13</sup>C NMR (126 MHz, DMSO-d<sub>6</sub>)



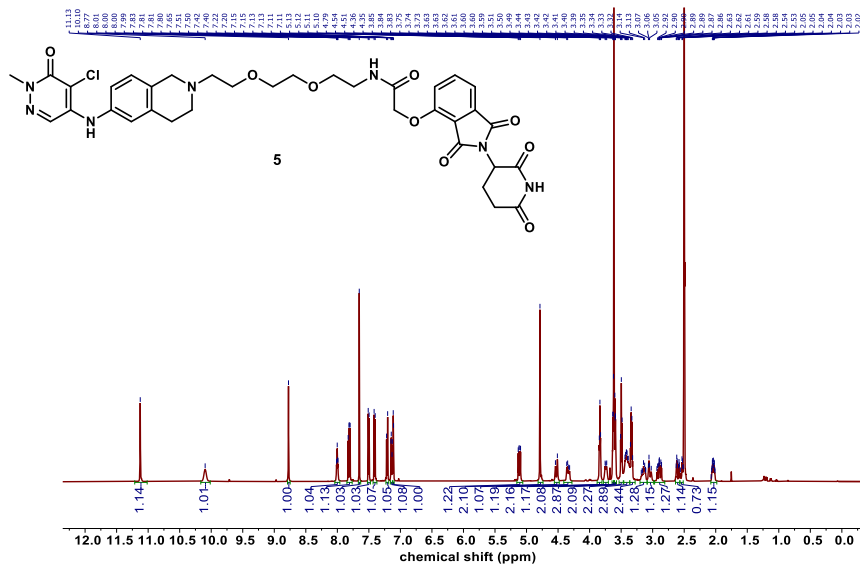
4, <sup>1</sup>H NMR (500 MHz, DMSO-d<sub>6</sub>)



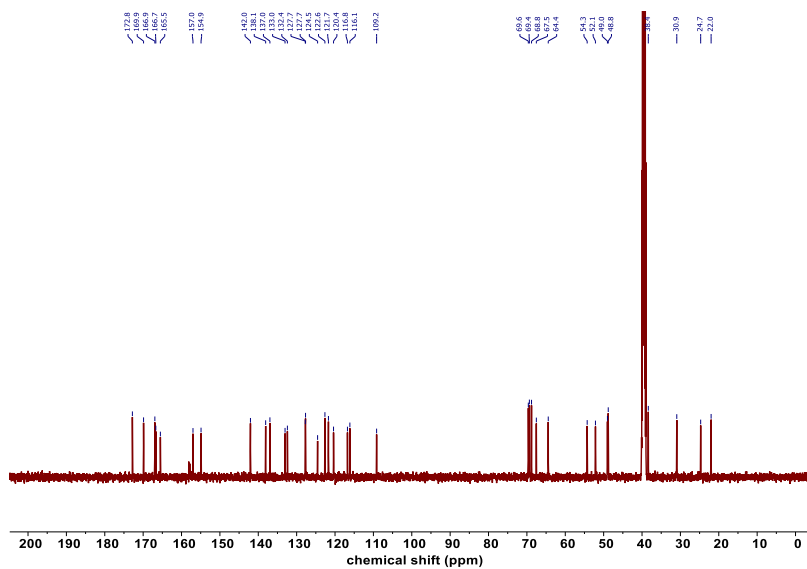
4, <sup>13</sup>C NMR (126 MHz, DMSO-d<sub>6</sub>)



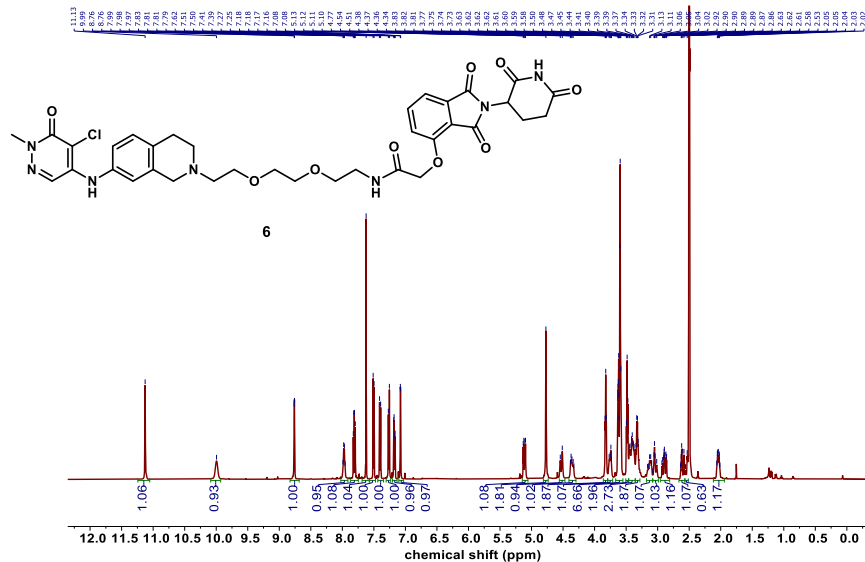
5, <sup>1</sup>H NMR (500 MHz, DMSO-d<sub>6</sub>)



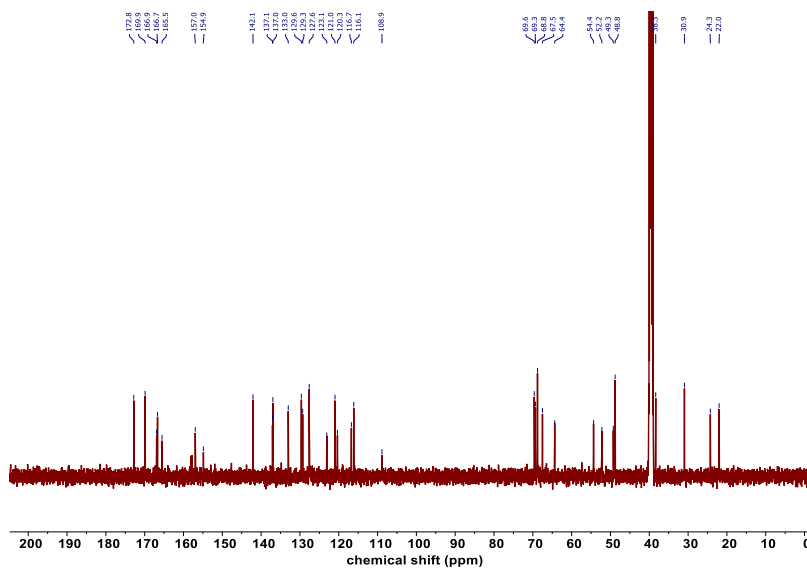
5, <sup>13</sup>C NMR (126 MHz, DMSO-d<sub>6</sub>)



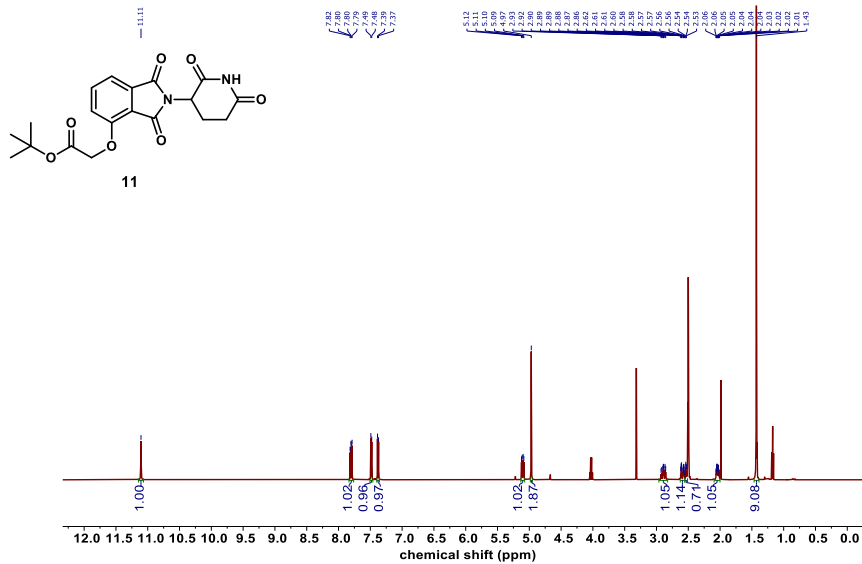
6,  $^1\text{H}$  NMR (500 MHz,  $\text{DMSO-}d_6$ )



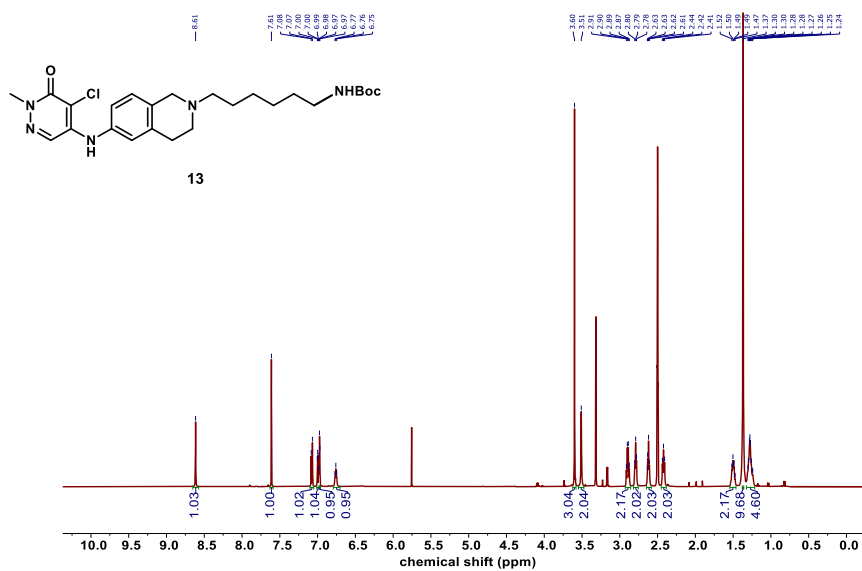
6,  $^{13}\text{C}$  NMR (126 MHz,  $\text{DMSO-}d_6$ )



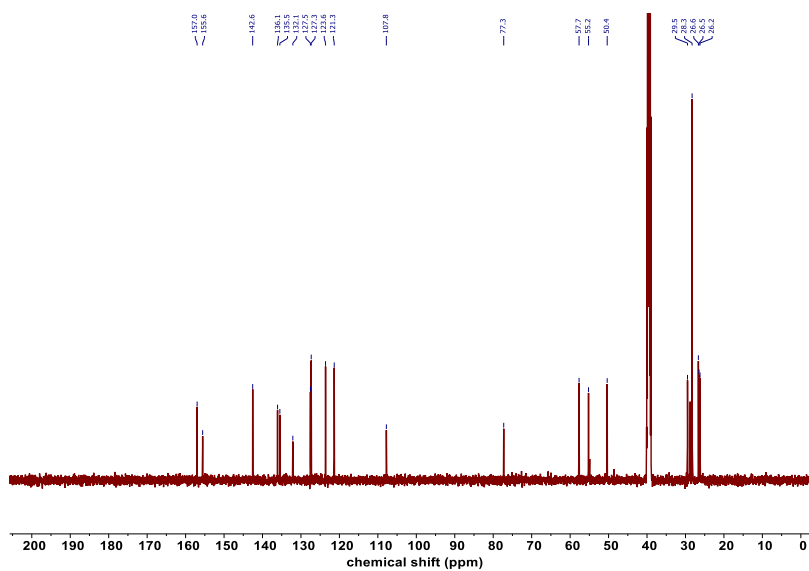
11, <sup>1</sup>H NMR (500 MHz, DMSO-d<sub>6</sub>)



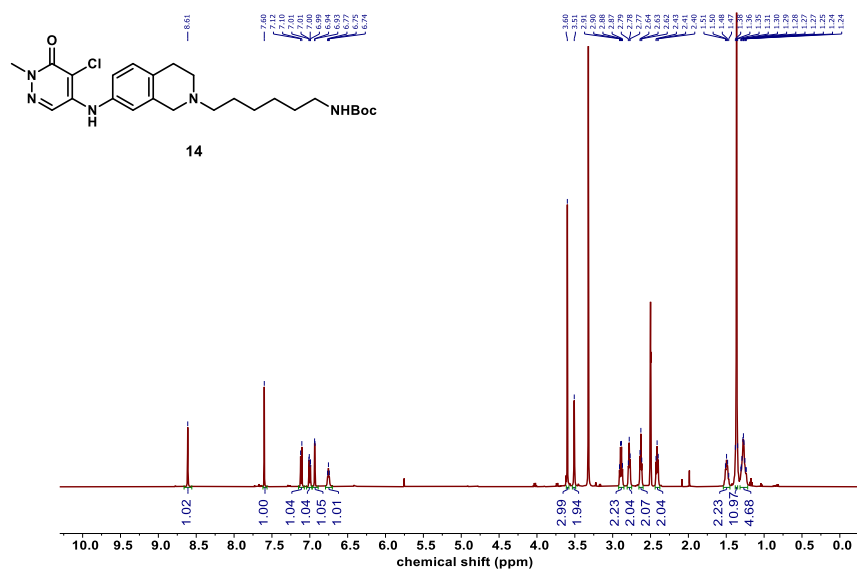
13,  $^1\text{H}$  NMR (500 MHz,  $\text{DMSO-}d_6$ )



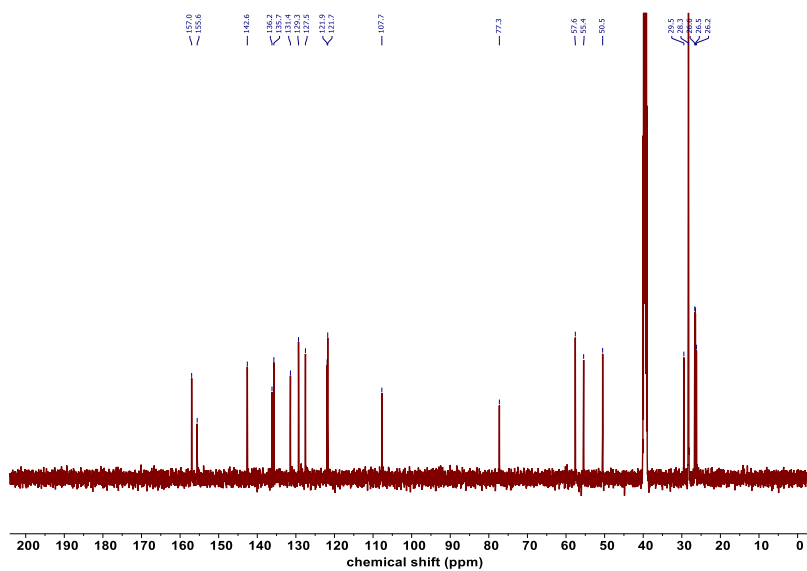
13,  $^{13}\text{C}$  NMR (126 MHz,  $\text{DMSO-}d_6$ )



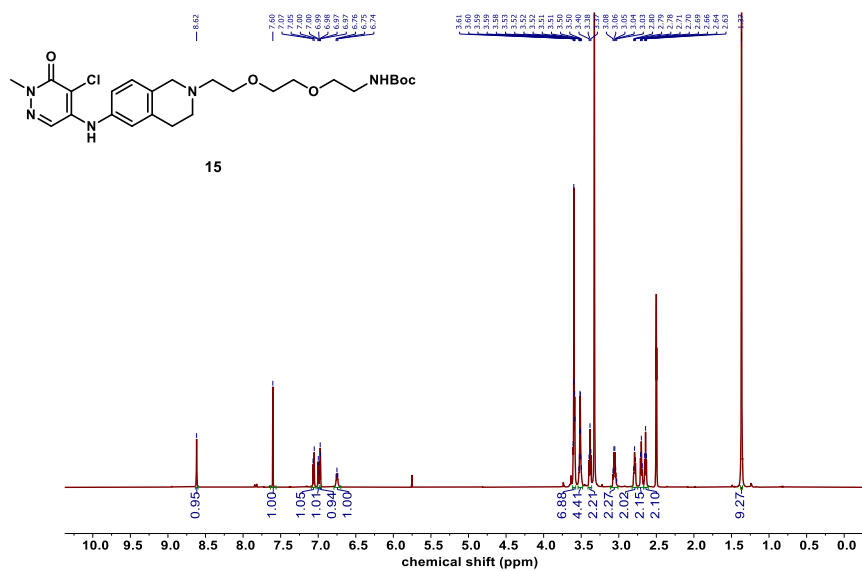
14, <sup>1</sup>H NMR (500 MHz, DMSO-d<sub>6</sub>)



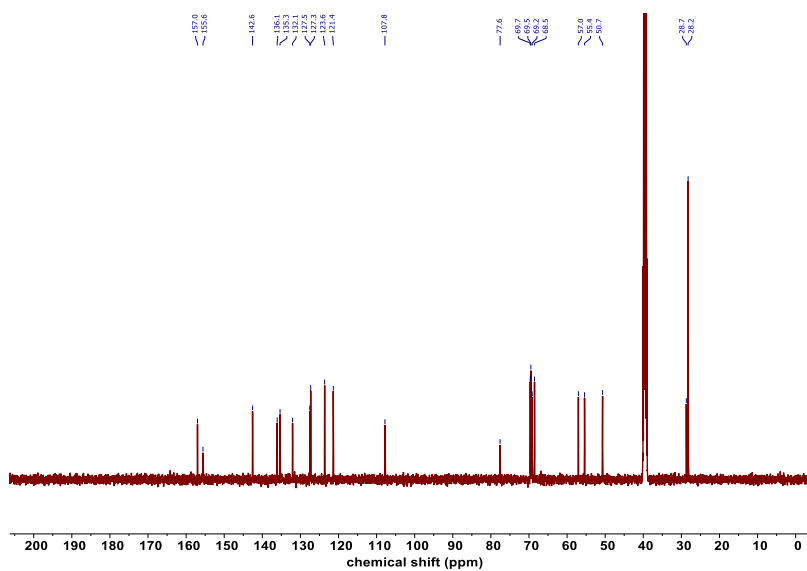
14, <sup>13</sup>C NMR (126 MHz, DMSO-d<sub>6</sub>)



15, <sup>1</sup>H NMR (500 MHz, DMSO-d<sub>6</sub>)

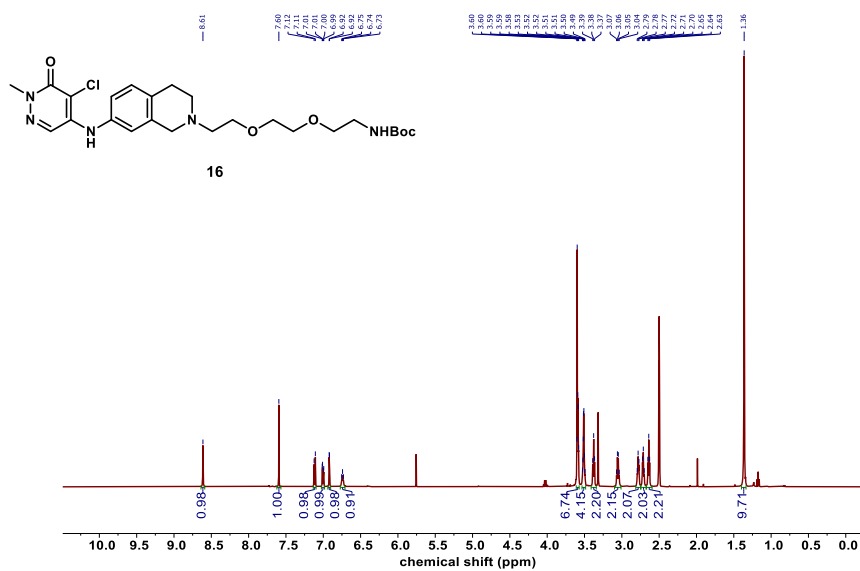


15, <sup>13</sup>C NMR (126 MHz, DMSO-d<sub>6</sub>)

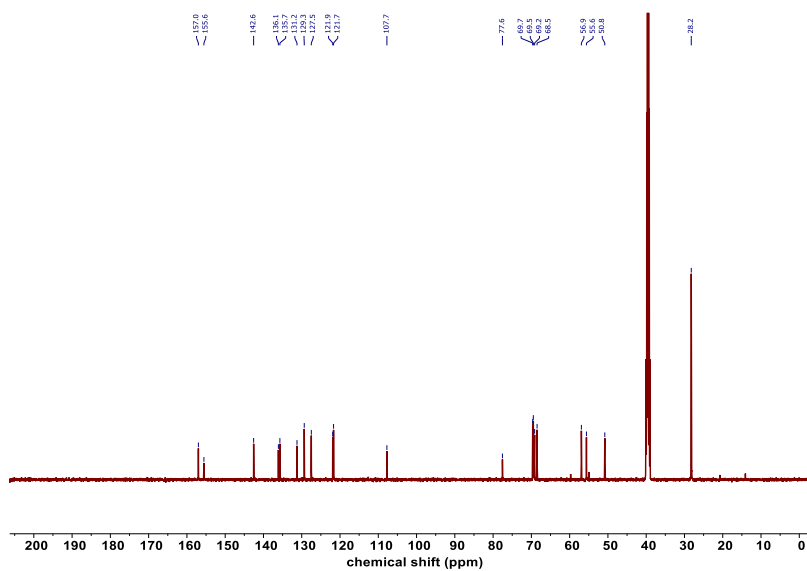




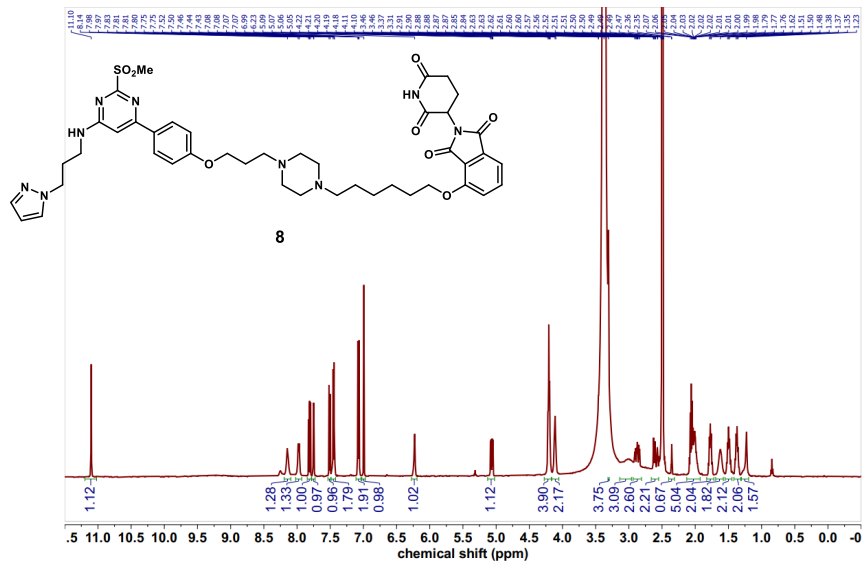
16, <sup>1</sup>H NMR (500 MHz, DMSO-d<sub>6</sub>)



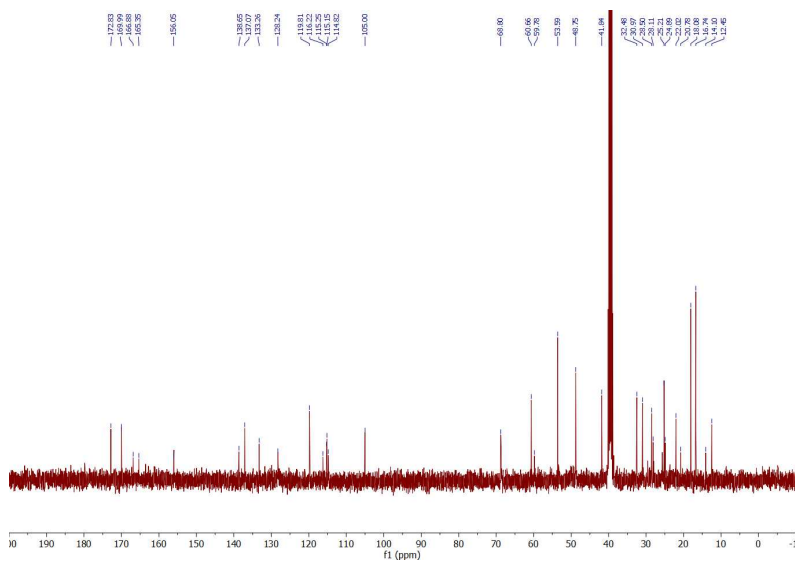
16, <sup>13</sup>C NMR (126 MHz, DMSO-d<sub>6</sub>)



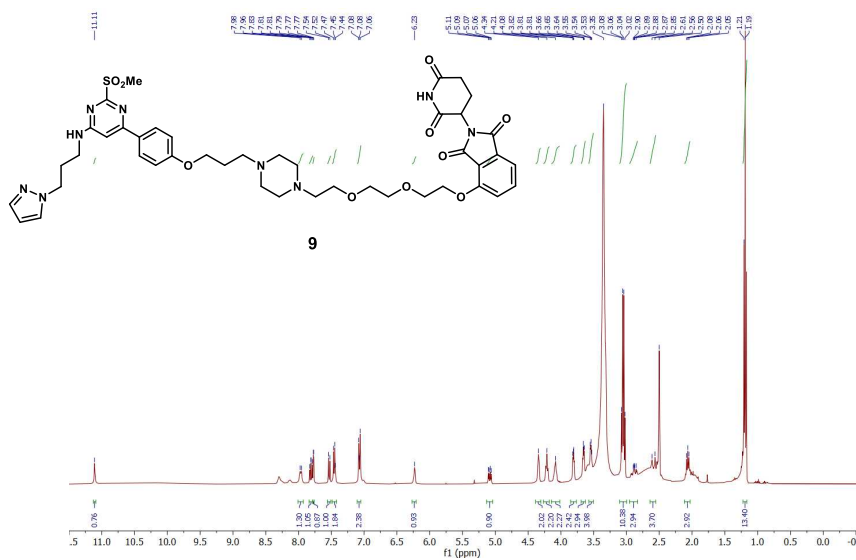
**8**, <sup>1</sup>H NMR (400 MHz, DMSO-d<sub>6</sub>)



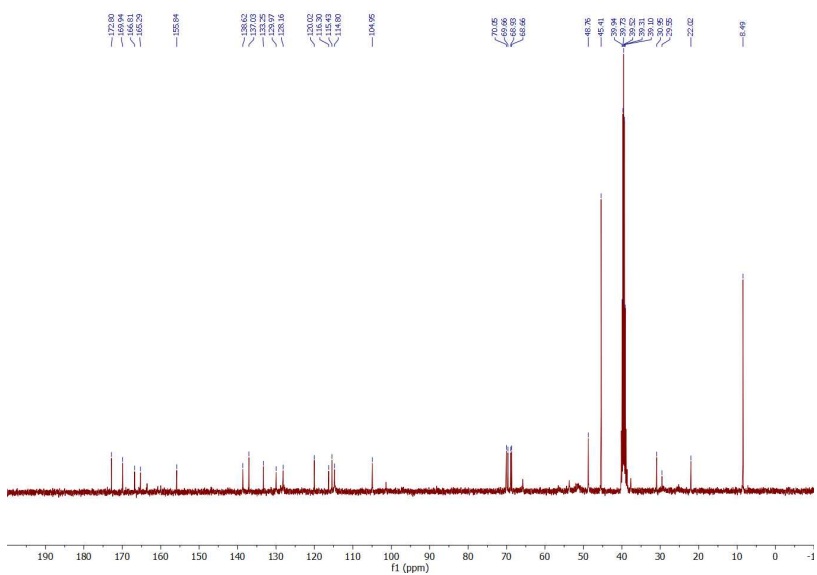
**8**, <sup>13</sup>C NMR (100 MHz, DMSO-d<sub>6</sub>)



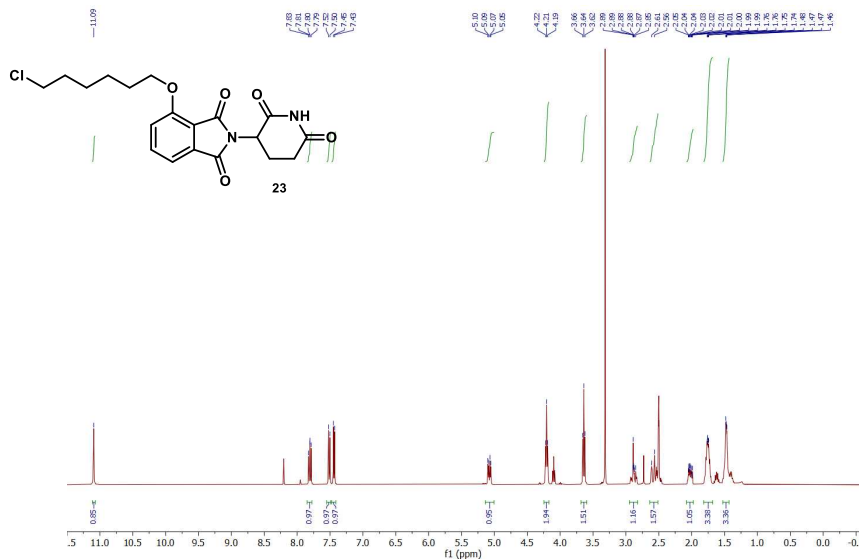
9, <sup>1</sup>H NMR (400 MHz, DMSO-d<sub>6</sub>)



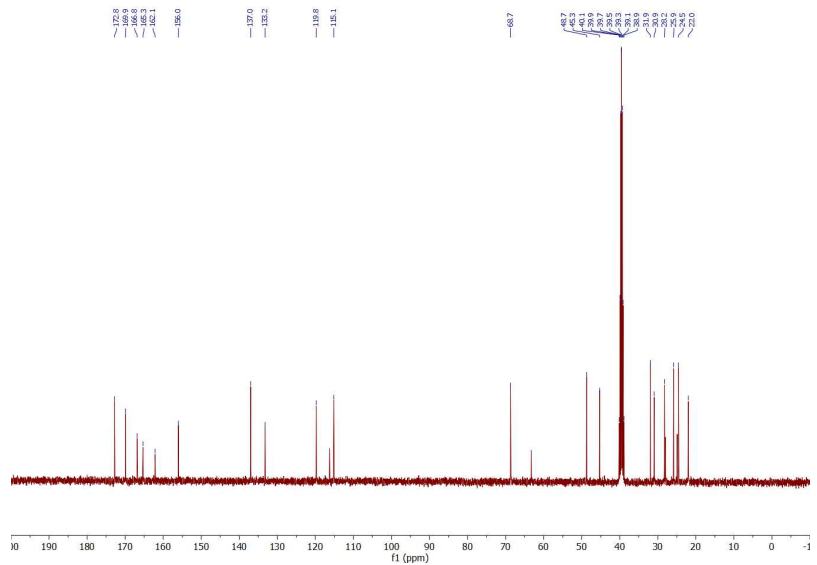
9, <sup>13</sup>C NMR (400 MHz, DMSO-d<sub>6</sub>)



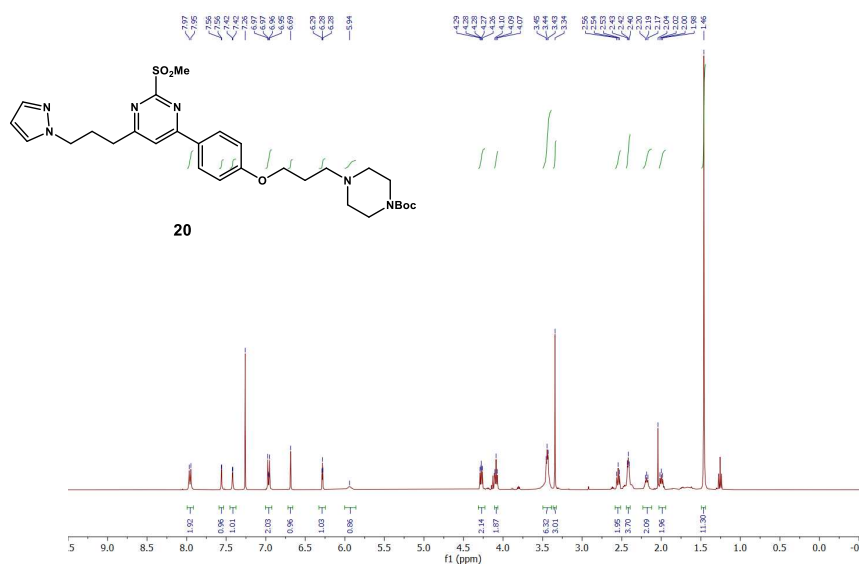
23, <sup>1</sup>H NMR (400 MHz, DMSO-d<sub>6</sub>)



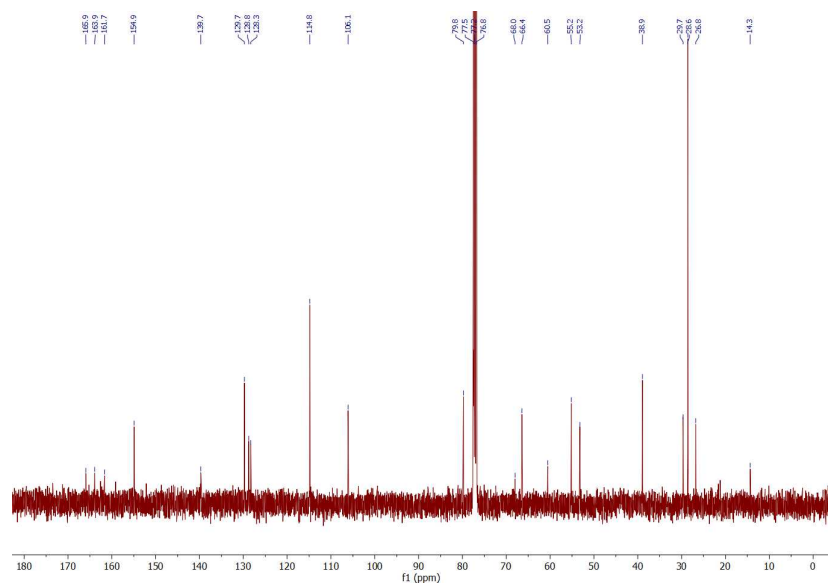
23, <sup>13</sup>C NMR (100 MHz, DMSO-d<sub>6</sub>)



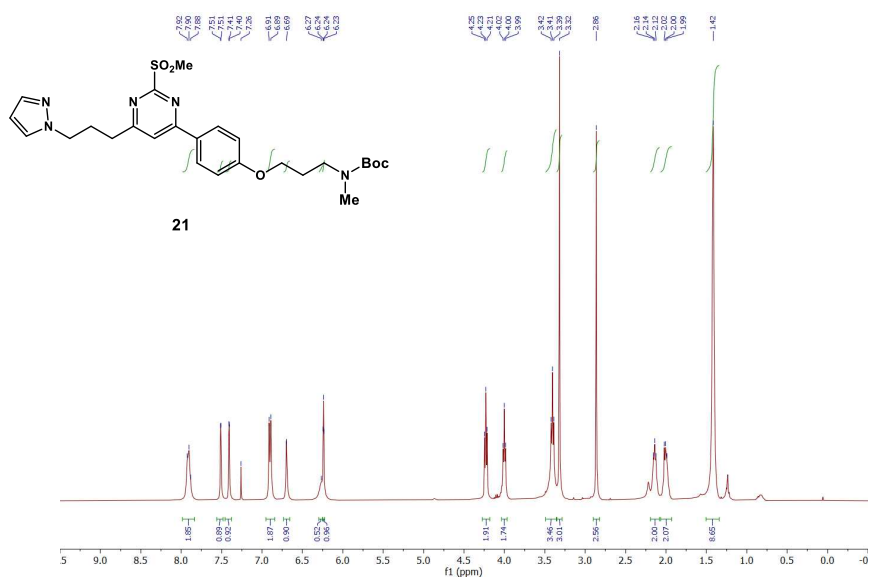
20, <sup>1</sup>H NMR (400 MHz, CDCl<sub>3</sub>)



20, <sup>13</sup>C NMR (100 MHz, CDCl<sub>3</sub>)



**21**,  $^1\text{H}$  NMR (400 MHz,  $\text{CDCl}_3$ )



**21**,  $^{13}\text{C}$  NMR (100 MHz,  $\text{CDCl}_3$ )

